Selective Laser Re-melting

Sonia Chung

A thesis submitted to
Auckland University of Technology
in partial fulfilment of the requirement for the degree of
Master of Engineering (ME)

2017

School of Engineering

Abstract

The additive manufacturing (AM) industry is heavily employed in a wide variety of applications today. Initially, the different processes have been used for concept modelling and rapid prototyping but are now capable of building fully functional parts. Selective laser melting (SLM) is one of the rapidly growing technologies since its inception in early 2000s. It creates parts by melting powder materials in layers using a laser heat source based on the information provided by a three-dimensional computer-aided design model. The parameters of SLM have been continuously optimised while attempting to produce fully dense parts comparable to the traditionally counterparts. This is an ongoing area of research due to the considerable number of variables involved in the process, including but not limited to powder material properties (powder deposition, particle morphology, particle size, particle size distribution and particle porosity), laser parameters (laser power, laser scan speed and laser scan spacing), and build chamber conditions (atmosphere, powder bed temperature and substrate plate preheating).

Selective laser re-melting (SLR) is yet another approach visualised for improving the quality of SLM parts by integrating the laser surface re-melting (LSR) schemes into the SLM process planning. By re-melting every layer of a part, improved mechanical and physical properties can be obtained through decreased porosities. The re-melting process promotes grain refinement with a larger temperature gradient and balling within solidified layers is reduced leading to the reduction of pores and defects. However, the SLR technique further complicates the small SLM process window and requires careful selection of parameters for

a successful build. Additionally, past SLR experiments employed laser powers less than 100 W as were made available with the older SLM machines.

This study explores the effects of laser re-melting in SLM with varying energy density settings, establishing the process to structure and the structure to property relationships. Laser powers up to 375 W are used, with appropriate laser scan speed settings, ensuring the minimum energy densities as required for the laser melting of 316L stainless steel powders. Microstructural analyses are performed on the cross-sectional areas of the parts evaluating the formation of melt pools and the structures within. Both mechanical and physical properties including surface roughness of the top and the lateral faces, hardness, tensile strength, and density are the critical responses measured and analysed based on experimental conditions with varying levels of laser re-melting. Other aspects such as the laser scan strategies and the build orientations are also given due considerations in the experimental designs.

All the experiments are conducted on the Renishaw laser melting system. One of the main problems faced is that the re-melting approach led to excessive heating, bubbling and loss of the layer structures when attempted at the same original density levels as required for the first pass. This has led to limiting the energy densities in the repeated passes at either a half or a quarter of the original energy density level. Certain improvements are noticed from the laser re-melting process, though the end results are the combined effects of a number of factors.

Table of Contents

List of Figures

List of Tables

List of Abbreviations

AISI	American Iron and Steel Institute
AM	Additive manufacturing
CAD	Computer-aided design
CW	Continuous wave
d	Laser scan spacing
D_L	Diffusion coefficient
e	Layer thickness
ED	Energy density
EDM	Electrical discharge machining
G_L	Laser melting temperature gradient
GTAW	Gas tungsten arc welding
HAZ	Heat-affected zone
HRB	Rockwell hardness B
HRC	Rockwell hardness C
ICSN	Intragranular cellular segregation network
LSR	Laser surface re-melting
LMZ	Laser-melted zone
LOM	Light optical microscope
M_a	Actual mass
M_{th}	Theoretical mass
Nd:YAG	Neodymium-doped yttrium aluminium garnet
P	Laser power
PMZ	Partially melted zone
R	Growth rate

R_a	Arithmetic average surface roughness
R_q	Root mean squared surface roughness
R_t	Total surface roughness
R_z	Ten-point mean roughness
SEM	Scanning electron microscope
SLM	Selective laser melting
SLR	Selective laser re-melting
UTS	Ultimate tensile strength
v	Laser scan speed
Yb:YAG	Ytterbium-doped yttrium aluminium garnet
ΔT	Solidification undercooling

Attestation of Authorship

I hereby declare that this submission is my own work and that, to the best of my knowledge and belief, it contains no material previously published or written by another person (except where explicitly defined in the acknowledgements), nor material which to a substantial extent has been submitted for the award of any other degree or diploma of a university or other institution of higher learning.

Acknowledgements

First and foremost, I would like to express my sincere appreciation and gratitude to my primary supervisor, Dr. Sarat Singamneni, for his guidance and knowledge during my time at Auckland University of Technology in completing the Master of Engineering. I am grateful as he has consistently supported and encouraged me in every aspect of my life from my undergraduate studies to my time as a research assistant and now, my postgraduate research. I am very appreciative of the numerous opportunities he has provided me throughout the years. I am also thankful to Professor Thomas Neitzert for being the secondary supervisor.

I am also indebted to all the laboratory and workshop technicians at AUT. I would like to thank Jim Crossen (technical services manager), Mark Masterton, Ross Jamieson for their immeasurable patience and assistance in mechanical testing, mounting / polishing and operating LOM. I would also like to thank Sonya Popoff (laboratory manager) and Yan Wang (laboratory officer) for their assistance in the science laboratory where I was able to safely perform chemical etching. Finally, I would like to show my gratitude to Ross Jacobs (3D printing lab - SLM), Patrick Conor (senior research officer – SEM) and Yuan Tao (SEM technician) for accommodating me and my research needs into their busy schedules.

I am also very grateful to all the fellow postgraduate students I have met along the way, for help, support and insight into the additive manufacturing industry. I was fortunate to work alongside fellow students with vast experience and knowledge in the field, as well as relentless work ethic.

Finally, I would like to acknowledge my friends and family. I am grateful for my powerlifting family at GetStrength for creating such an awesome environment to train in every single day. Also, a special thanks goes to John, for believing in me from the start, for the never-ending words of encouragement and for making every chapter of my life so wonderful. My greatest gratitude goes to my mum, Grace, for her unconditional love, my sister and best friend, Jenny, for her unflagging support, advice and wisdom, my cousin, Lindsey, for the tremendous amount of support from the other side of the world, and the rest of my family in South Korea and United States of America.

Chapter 1
Introduction

1.1 Selective laser melting

Additive manufacturing (AM) has evolved from the rapid prototyping processes and became an essential and important avenue in modern manufacturing, considering the ability to produce complex components with high dimensional qualities. The demand and interest in AM technology grew significantly in recent years due to the many competitive advantages such as the high degree of geometrical freedom, shorter manufacturing times from design to the final product, and material flexibility. Nowadays AM processes are used in a wide range of applications, fabricating fully functional parts. Medical field, military aerospace, alternative energy, semiconductor, packaging, and hybrid manufacturing are common industrial sectors employing AM.

Selective laser melting (SLM) is one of the versatile AM processes which uses a laser heat source to melt layers of powder metals. Considering the abilities to convert powder metals into finished forms directly from CAD data, this technology is currently attaining significant research and commercial attention. Being an additive process, the material wastage is minimal, where the unused powder is recycled for future builds. Further, the layer by layer fabrication allows for more complex shapes to be built with no special tooling requirements.

Considering the powder material consolidation by a fast moving laser energy source, numerous process related issues arise in SLM such as chamber atmosphere, preheating of substrate plate, layer thickness and build orientation. Further, laser parameters such as beam size, power, scan speed and spacing, and scan strategies become important. Commercial metal systems currently available for processing by SLM include specific alloy of stainless steel, cobalt chrome, titanium, Inconel, and aluminium. The process conditions often lead to complex micro and meso structures based on the process parameter combinations used.

Metallographic evaluation is crucial when studying the quality of metal SLM parts as the localised melting and rapid solidification leads to non-equilibrium phases and changes in the microstructural features. The resulting melt pool geometry, grain growth, and sizes aid in parametric analyses also. Mechanical and physical properties are highly dependent on the metallography of SLM parts and may differ to those produced by conventional production techniques. Due to the nature of the line-by-line and layer-by-layer material consolidation in SLM, any defects and imperfections in a layer will affect the subsequent layers and eventually the overall part quality. Hence it is important to use the most appropriate combination of the critical process parameters in order to achieve full density.

One of the major shortcomings with SLM is the presence of porosity related defects and imperfections. Uneven thermal stressing may also lead to internal stresses, warping and dimensional inaccuracies. The primary cause of porosity is the balling phenomenon where metal agglomerates are formed on the layers during the build. This prevents the new layer of powder to spread sufficiently over

the part and the laser beam is unable to penetrate through the previous layer, leaving areas free of the material. Thermal loading also leads to yet another form of porosity in SLM parts, cracks resulting from the high internal stresses, especially near the melt pool borders.

Past research evaluating the porosity issues in SLM are mainly focussed on understanding the roles of different process parameters both individually and combined and optimising combinations of them to achieve the best densities. Further, the interactions between critical process parameters are also evaluated and overall, it was shown on numerous occasions that fully dense parts can be obtained with different metal systems processed by selective laser melting. However, the process parameter combinations must also be considered together with other variables such as the SLM system, the powder material composition and properties, and the intended application of the final product. In view of the need for the overall quality improvement, specific solutions are also attempted targeting better consolidation of the powder substrates into solid layers and subsequent inter-layer coalescence.

1.2 Selective laser re-melting

Selective laser re-melting (SLR) is one of the attempts in these lines, which evolved through combining the SLM layer formation with the laser surface re-melting methods. Laser surface re-melting is normally used with processes such as laser cladding, and involves reheating and repair of the top surface, by repeating the laser heating of the surfaces of the part. It was reported to achieve

significant improvements in the surface quality as a result of the full consolidation of material in the top layer. The melt pools and heat affected areas emanating from laser surface re-melting are similar to those observed in laser welding methods.

In the context of SLM, while scanning atop each layer, the laser interaction is similar to the welding process, but becomes more complex due to the particle-by-particle welding, heat affected jones spreading all over, and the subsequent effects across the multi-layers. Combining the laser re-melting to the formation of every layer in the SLM build mechanisms is expected to improve the intra-layer consolidation, leading to better overall part density levels.

Research review suggests earlier attempts already made integrating the laser re-melting approaches with SLM. The results reported overall improvements, but the laser melting systems used were of the old generation. The laser power employed was quite low and build atmosphere is different to the current methods employed. Considering the significant improvements predicted to be possible, it is important that the selective laser re-melting approach be further investigated based on the current SLM systems with higher laser energy options and better build chamber environments. The current study is an attempt in this direction and a Renishaw AM250 system is used to revisit and review the effects of laser re-melting with stainless steel powders.

1.3 Research objectives

The research design and methodology are developed to evaluate the plausible roles of re-melting each layer with varying energy density conditions while selective laser melting the stainless steel 316L powders. The following are the main objectives:

- Assess and understand the background of SLM in metal AM industry.
- Identify the current major issues of SLM with 316L stainless steel and review previously attempted methods and recent studies attempting improvements.
- Explore the effects of laser re-melting during selective laser melting of 316L stainless steel with varying energy density (ED) settings and build orientations using a modern Renishaw SLM system with higher laser powers and an argon atmosphere in the build chamber.
- Establish the process, structure, and property relationships in SLM integrated with laser re-melting.
- To determine the difference between SLM and SLR 316L stainless steel, if any, and conclude whether SLR is a feasible alternative solution to SLM.

1.4 Thesis layout

The literature review of SLM begins in Chapter 2 with the focus on the fundamentals of SLM process and parameters in general and then the laser melting of 316L stainless steels and associated quality aspects in particular.

Current literature on the use of laser re-melting in SLM is paid some attention next. The research gap and the questions are identified next, leading to the identification of the methods. The experimental methods are explained in the later part of Chapter 2 together with the characterisation of the 316L powder materials used as the experimental materials for the current experimental research.

The process-structure relationships are evaluated in Chapter 3 including the analysis of melt pools and the microstructural features of SLM 316L stainless steels with and without laser re-melting. The process-property relationships are characterised in Chapter 4. Chapter 5 is a critical consideration of results from both structure and property characterisations and a discussion integrating the results. Critical conclusions are drawn and listed in Chapter 6.

Chapter 2

Literature Review, Research Gap and Questions

2.1 The laser melting process

Selective laser melting is a developing additive manufacturing technology that involves melting of powder material in layers using a laser to create three-dimensional parts. As depicted in **Fig. 2-1**, the SLM process begins with the design of the build through computer-aided design (CAD) where the information is transferred to the machine which creates the part on a build platform. Sufficient powder deposition is required between every layer in order to provide the necessary amount of material that is spread homogeneously throughout onto the substrate plate and powder reservoir. The effects of continuously recycling unused powder is just beginning, but yet to be explored. This process is heavily influenced by its parameters such as: laser power, laser scan rate, laser scan spacing, powder bed temperature, preheating of powder metal / substrate plate, and atmosphere of the build chamber. The designing and selecting appropriate parameters for each build are of paramount importance. During the build process, the powder material is solidified in layers and must be melted sufficiently in order to adhere to the previous layer. However, there are possibilities of not heating the material adequately which will not allow the layers to consolidate, or overheating and therefore deteriorating the material. Finding the perfect combination of

process parameters for various materials, shapes / sizes of parts and their applications is a challenge which the AM field is currently facing [1].

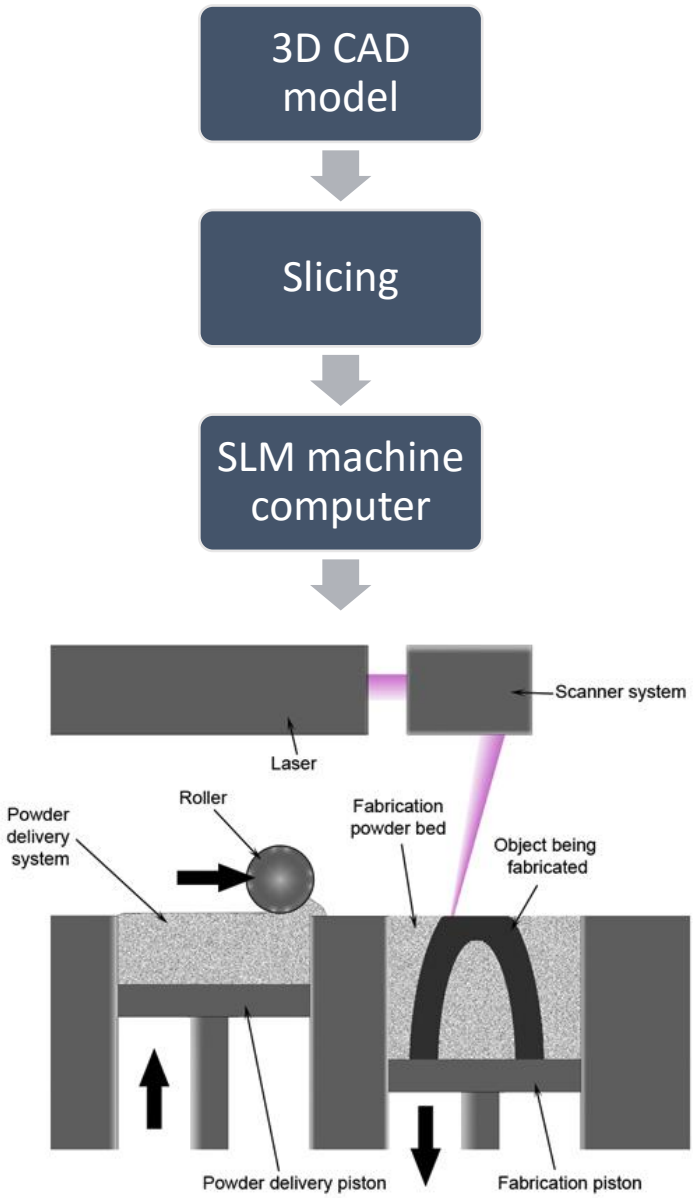

Fig. 2-1 – Schematic representation of selective laser melting

SLM has shown potential for replacing the current bulk material production methods in specific cases in terms of fully dense parts, reduced number of parts and reduced post processing. There are numerous advantages presented by SLM which may benefit the manufacturing industry immensely and hence has

been recognised as a technology worthy of investment in research and development. For future commercial use, studies have produced tools to optimise the SLM production process such as dimensional analysis for process control [2], particle packing simulation [3, 4] and cost-model to manufacture parts more economically [5].

The methods of producing the desired outcome of SLM, in order to achieve an equal or higher level of quality compared to products of conventional manufacturing methods, have been explored extensively since the early years. Many studies have analysed the effects that various SLM parameters and processability of powder materials have on the build [6-9]. The SLM build characteristics such as the types of single tracks (continuous with a crescent / elliptical cross section, irregularly broken, balled, only partially melted) [10], surfaces (balling / rough surface, well connected / fine surface, not connected) [11] and the microstructural changes [12-15] are observed to investigate the quality of parts. The aforementioned SLM build characteristics have direct consequences on the mechanical and physical properties of the part such as surface quality [10, 11, 16-21], hardness [16, 19, 22], tensile strength [23-31] and density [20, 32]. Many studies used energy density to define the energy supplied by the laser per cubic millimetre of powder material in unit time when performing parametric analyses. This is determined using **Eq. 2-1**:

$$ED = \frac{P}{vde} \text{ [J/mm}^3\text{]} \quad \text{.....Eq. 2-1}$$

where P is laser power, W, v is laser scan speed, mm/s, d is laser scan spacing, mm and e is layer thickness, mm [33].

The amount of energy density was found to have an effect on the hardness of SLM parts where there is a specific range of energy input for each material which gives the highest microhardness values. Hardness also improves with re-melting of the solidified layers whether it is done by laser surface re-melting (LSR) or selective laser re-melting (SLR) as it is a form of heat treatment of the material. Due to the nature of the SLM process, it was recognised that the conventional post processing procedures could be minimized, if not avoided completely which would benefit the overall cost of manufacturing. One of the aspects was the surface quality of an SLM part where it is affected primarily by laser power, laser scan speed [16], laser scan spacing [18, 19] and build orientations [17, 21], while on the contrary, laser exposure time was found to have a minimal effect on the surface roughness. The deterioration of surface quality, which is caused by pool solidification and shrinkage, promotes poor powder deposition. As a result, rougher surfaces will form on the consequent layers [34]. Using a medium laser power of 98 W and low scan speed of 200 mm/s produced the lowest surface roughness results, yielding an improvement of approximately 90 %, and the re-melting technique was also reported to have a similar positive effect which improved the surface quality significantly [16, 20, 21]. In terms of ED, the lowest surface roughness was obtained at an energy input of 125.4 J/mm^3 using a maximum laser power of 200 W [19]. A poor surface roughness will require post processing due to poor dimensional accuracy.

SLM products were tested using various methods according to the specifications and the applications in each case. In order for SLM parts to replace the current readily available tools and materials, the quality and hence the performance of

the parts were to surpass the latter. Numerous studies reported equal or greater tensile properties of SLM parts compared to the conventional material processing methods [23, 26, 27, 31]. Also, some found the build orientation in SLM builds did not seem to have a great impact on the tensile properties [23, 27]. On the contrary, some studies found that parts built at an angle of 45° consistently performed worse than those built at an angle of 0° or 90° [24, 31] which they concluded was due to the solidified layers creating a 'staircase formation' causing discontinuous grain growth in all three axes as shown in **Fig. 2-2** [35]. Grain growth varied with the different build orientations where anisotropy in the 45° parts gave poor results in tensile strength. Moreover, in the worst cases, it showed significant deterioration in the mechanical and geometrical properties as a result of delamination of the layers. This was evidently the opposite of the horizontal samples with superior tensile properties where the direction of load was parallel to the layers but perpendicular to the continuous epitaxial columnar grains within the microstructures. Other supportive aspects are longer inter-layer time intervals which increase the cooling rates and leading to finer microstructures. Additionally, the application of high preheating temperature to the substrate plate also proved to be beneficial as the technique aids in producing almost fully dense parts, despite the quality of the material decreasing in areas furthest from the substrate plate. These are highly desirable outcomes in terms of tensile properties in SLM.

Considering the number of variables and the required precise process windows, it is probable that the products of SLM will have some sort of minor defects and imperfections. Inappropriate application of the laser heat source to the powder bed material is the main cause of unwanted residual stresses due to the heating and cooling cycles the material undergoes. This results in distortion and even

delamination of the final product. Furthermore, this is difficult to control with varying part dimensions and shapes. Components with complex geometries are likely to experience a wide range of residual stresses that may be undesirable depending on the functional purposes [36]. Moreover, the laser scan speed has a tremendous impact on the density of the part. Depending on the laser power combined with laser scan speeds, instability in molten pools may occur. This results in spheriodisation where too high and too low laser scan speeds will cause shrinkage induced balling and splashes induced balling, respectively [6, 11]. Either of the balling effects will contribute towards internal porosity, hence reducing the part density. A similar phenomena called laser spatter occurs with the formation of oxide layers on the material which is dependent on the oxygen level of the build chamber. Laser spatter in SLM is caused by overheating of the melt pool and may be more detrimental than balling as the molten metal of spherical morphology may be deposited erratically onto any part of the build including the powder material [37]. Porosity evidently affects most physical properties such as hardness and tensile strength [19, 32].

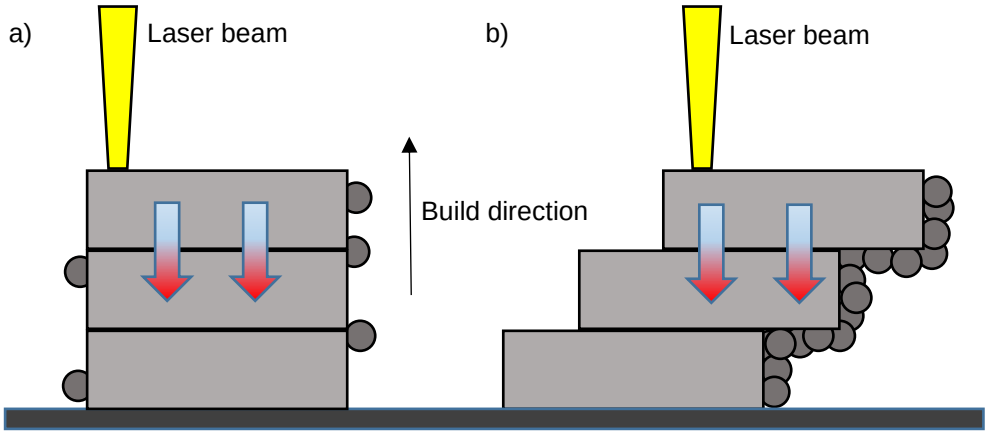

Fig. 2-2 - a) SLM build at 0° or 90°, b) SLM build at 45°

2.2 Critical issues and process enhancements in stainless steel SLM

The use of metal powders in additive manufacturing has been increasing exponentially due to the growing demand and interest in the industrial use of the process [38]. The capabilities of metallic parts produced by selective laser melting are widely acknowledged and used in a broad variety of applications. With the development of the SLM process and access to different types of metal powders, the parts are no longer produced solely for prototyping purposes. Common materials that can be used with various SLM systems include stainless steels, aluminium, nickel, cobalt-chrome and titanium alloys. The quality of the materials in the powder the form is crucial in SLM where thin, uniform layers are required for high quality parts. The key powder particle properties that can be evaluated are particle morphology, particle size, distribution and porosity. The methods in which the alloys are converted into the powder forms used in AM determine the particulate properties. This process is illustrated in **Fig. 2-3** where it features the most favoured method, the gas atomisation, with its advantages being wide range of alloys, range of particle sizes from 0 µm to 500 µm and spherical particles [39]. Different methods of sourcing the powder material are aspects of the manufacturing process when considering factors outside of the build, such as costs. Powder materials can be purchased through suppliers direct from powder manufacturers, machine manufacturers or from validated third party suppliers where the main differences between the methods of sourcing the powder material are compatibility of materials to machines, ease of sourcing and reliability in terms of powder specifications and support with possible build failures. With the growth in the AM industry, the supply chain of materials is also expected to grow through

improvements in powder production and / or optimisation of the current supply chains.

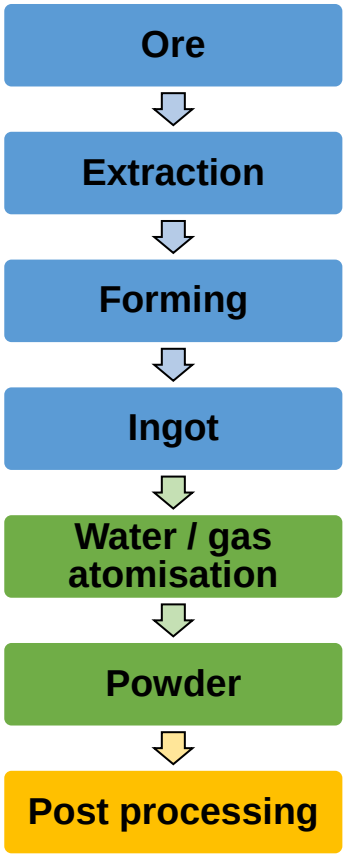

Fig. 2-3 - Metal powder production steps flow chart

Metal AM has many applications from rapid prototyping to functional parts in medical, automotive and aerospace industries. It offers many advantages over traditional manufacturing methods. The main advantage of SLM is having no limitations on part geometry as SLM builds occur directly from three-dimensional CAD models. Not only is it capable of producing complex shapes that were previously extremely difficult, if not impossible, but it provides the option of producing several parts of a component in one single build. While metal AM proves to be superior over a majority of manufacturing techniques, it has its disadvantages and is susceptible to defects. The current SLM process with metals cannot be used for mass production. The production of identical parts in

large quantities is within possibility in the near future, however, as the technology develops and process times are reduced.

One of the most common materials used for SLM is the stainless steel grade referred to as 316L as per the American Iron and Steel Institute (AISI) chemical compositions and mechanical properties. This is available in both gas and water atomized powder forms. Studying the effects of process parameters on 316L stainless steel powders has become a critical part of research in order to optimize physical properties and hence the part functionality. With a complete consolidation of powder material as an end goal of a successful build, parametric studies have concluded that laser power, laser scan speed and laser scan spacing are the most influential factors. A study also found that the gas flow within the build chamber had an influence on the mechanical properties but did not have a significant impact on porosity [40]. The various combinations of these process parameters produce a broad range of possible defects, while porosity is a major issue. This is revealed through observations of the cross sections of the SLM 316L stainless steel parts. The pores could appear as large gaps between the melt pools or as tiny micro-pores that are dispersed throughout the cross sectional area adversely affecting the physical properties and are therefore highly undesired.

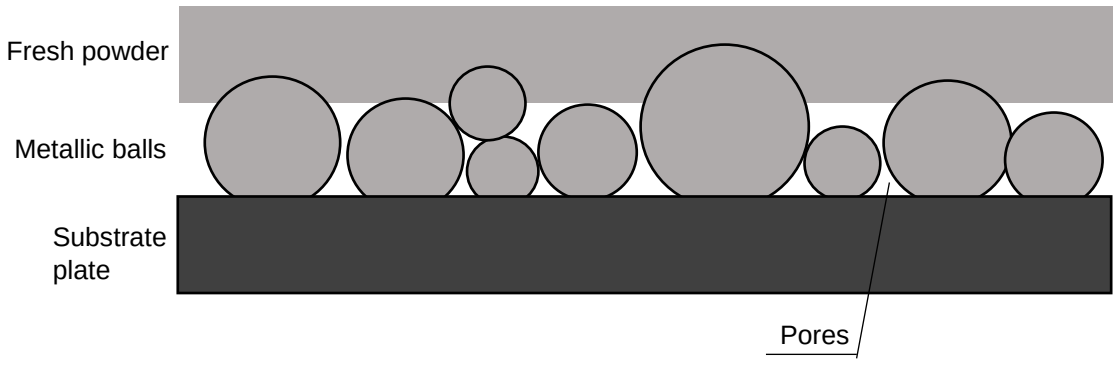

Fig. 2-4 - Balling induced pores

One of the major causes of open and trapped porosity in SLM 316L stainless steel parts has been identified as the balling phenomenon, as discussed previously. The metal agglomerates contribute greatly towards pore formation creating a rough surface. As illustrated in **Fig. 2-4**, a layer of powder material will fill the pores as it is rolled in preparation for the melting of the following layer [41]. However, depending on the laser parameter settings for the particular build, the ED may not be sufficient enough to penetrate the fresh powder that has filled the pore channels. This creates capillaries which affect the next layer and the process repeats itself in the formation of all subsequent layers. Cracks and micro-cracks have also been established as a result of the pore formation in SLM parts. The moving laser concentrating a high energy beam induces a great temperature gradient during the melting and solidification processes. This temperature gradient within the solidified metal leads to high internal stresses and contribute towards cracks and porosity. Such high volume of porosity corresponds to low density and consequently inadequate physical properties such as hardness and tensile strength [19, 32].

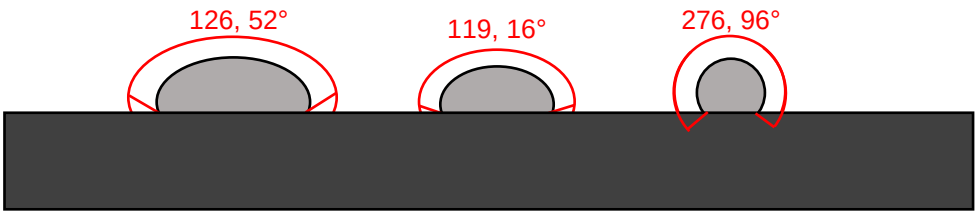

Fig. 2-5 - Cross-sections of single track scans illustrating contact angle

To prevent balling, which causes defects, detailed studies on single tracks and their capillary instability was carried out [27-29]. The shape of the single track determines the quality of SLM layers which enables each laser scan track and

consequent layers to consolidate sufficiently, producing a fully dense part. The ideal contact angle between the laser scan track and the substrate surface was identified as “Φ < 180° (less than half a cylinder)” where “the segmental cylinder had been stable at any length” [27]. With varying laser power, powder layer thickness, laser scan speed and substrate surface, cross sections of single track beads were observed for conformation with the contact angle, as shown in **Fig. 2-5**. Shape variations in single tracks were analysed with varying process parameters [34]. The width of a single track is directly proportional to the laser power, and hence the ED, which in turn would determine the scan spacing and overlapping rate. Depending on the ED settings and the width of the single track, the surrounding powder particles were blown away creating powder-free zones. In a standard SLM build, these powder-free zones from one laser scan track will affect the adjacent scan tracks. Therefore, surface roughness of SLM parts was identified as dependent on the width of a single track, one of the most important parameters.

Evaluation of the mechanism of formation of the laser scan track enables a deeper understanding of the formation of pores and types of single tracks. The formation mechanism of melt pool is quite complex due to the rate at which it occurs and the powder area scale that is affected in unit time. Khairallah *et al*. explored the strong dynamic melt flow in terms of the temperature and the velocity which cause porosity, spatter and denudation zones [42]. It was reported that the melting of the powder material occurs ahead of the laser beam and creates an indentation due to the recoil pressure. This recoil force, along with temperature, decreases exponentially once the laser beam passes the area. Consequently, the melt-flow velocity vector reverses within 5 μs and this abrupt change

increases the chance of trapped gas bubbles, creating pores within the melt pools. As the depression is filled, partially melted particles will flow in their preferred directions according to the Marangoni effect which will determine the shape of the scan track and hence the quality of the part.

Having recognised porosity as the main issue in SLM, many studies have assessed the effects of SLM processing parameters and build orientations in order to improve the part performance. As a part of a parametric study, predictive models were generated for physical and mechanical properties which illustrated the effects of individual factors using statistical analyses [33]. These results were combined to highlight the importance of the interactions within the process parameters when investigating the effects on SLM parts. Similarly, Dadbakhsh *et al*. investigated the effects of part layout, laser scan strategy, and gas flow direction in the build chamber on the quality of SLM parts [40]. In this study, all parts were built with a scan strategy in which the laser moves along the x- and the y-directions alternatively in successive layers. It was concluded that the physical and mechanical properties, such as porosity and tensile strength, were not affected by the part layout, whether they were oriented parallel or perpendicular to the gas flow.

Evidently, optimisation of process parameters, part orientation, and slicing or raster strategies are common methods employed to control the critical responses of selective laser melting. Considering the basic mechanism of the laser interaction forming each layer of the solid, inferences could also be drawn based on laser surface re-melting techniques as possible means of achieving improved layer formation. If each layer is formed better, the overall combination of the

layers within the solid will be better, thus leading to a fully dense consolidation of the powder.

Laser surface re-melting is a technique applied to parts produced by traditional means such as casting, in attempts to improve the quality of the surface layer. This is an adaption of laser surface alloying which is a material processing method that involves a laser heat source to create a metal coating by melting both the alloying element and the substrate surface [43], [44]. Laser surface alloying primarily aids in the corrosion resistance of stainless steel parts. Laser surface re-melting studies often compared the laser scan tracks and associated microstructural changes to those of welding by defining zones within the microstructures as: laser-melted zone (LMZ), partially melted zone (PMZ), heat-affected zone (HAZ), and the unaffected base material [45], [46]. In one particular study, welding method of gas tungsten arc welding (GTAW) was used to re-melt the surface of sintered steels which reduced surface roughness by eliminating open porosity [20]. LSR also resulted in significantly improving the corrosion resistance of the parts by forming a refined dendritic structure in the melted zone [45], [47].

Considering the beneficial roles of laser re-melting, laser surface re-melting approach was also attempted in selective laser melting. It is easy to implement and only needs an appropriate modification in the laser scan strategies, without any additional equipment or modification to the laser melting system. Up to three re-melting scans were achieved by Yasa *et al*. [16] using AISI 316L stainless steel and a continuous neodymium-doped yttrium aluminium garnet (Nd:YAG) laser with a wavelength of 1064 nm. All samples were built with the same parameters:

a laser power of 105 W, a scan speed of 380 mm/s and a scan spacing of 125 µm. The re-melting parameters varied with each sample with laser powers ranging from 85 W to 105 W, laser scan speeds ranging from 50 mm/s to 200 mm/s and scan spacing ranging from scan spacing factor of 5 % to 20 %. Through image analysis of sample cross-sections, they concluded that higher energy density settings, high laser power or low scan speed, samples obtained greatest amount of porosity. The porosity in these samples were worse in those with multiple re-melting scans despite a significant improvement from no re-melting. Small scan spacing factor of 5 % also resulted in higher porosity. In terms of microstructural features, they discovered that more re-melting laser scans produce a finer lamellar structure as overlapping scan tracks merge to form straight lines. The corresponding melt pools consist of refined cellular / dendritic structure with a cell size smaller than 1 µm.

Not only is LSR generally used to enhance the quality of top surfaces, but inclined and / or curved surfaces also, as they are an arrangement of the staircase formation, which was introduced in the previous Section 2.1 (**Fig. 2-2b)**). The severity of the staircase effect is dependent on the combination of the inclination angle and layer thickness. When the contours of SLM AISI 316L stainless steel parts with inclined surfaces of angles varying from 10° to 70° were re-melted, both average roughness (R_a) and total roughness (R_t) were reported to have improved most for lower laser scan speeds [48].

It has been established that instability in melt pool formation, shape of laser scan tracks and balling during SLM builds causes both porosity, as discussed previously, and surface roughness [49] due to a great variation in surface profile.

While careful selection of parameters is required for SLM, the build design is a much more delicate process in SLR. When appropriate re-melting was applied to every layer of SLM parts (**Fig. 2-6**), the manufacturing time increased but mechanical and physical properties were reported to have improved [34]. The reduction of defects, elimination of micro-pores and improvements in the surface quality were direct results of SLR, wherefore the hardness, tensile and fatigue strengths, wear, thermal and electrical conductivity were enhanced.

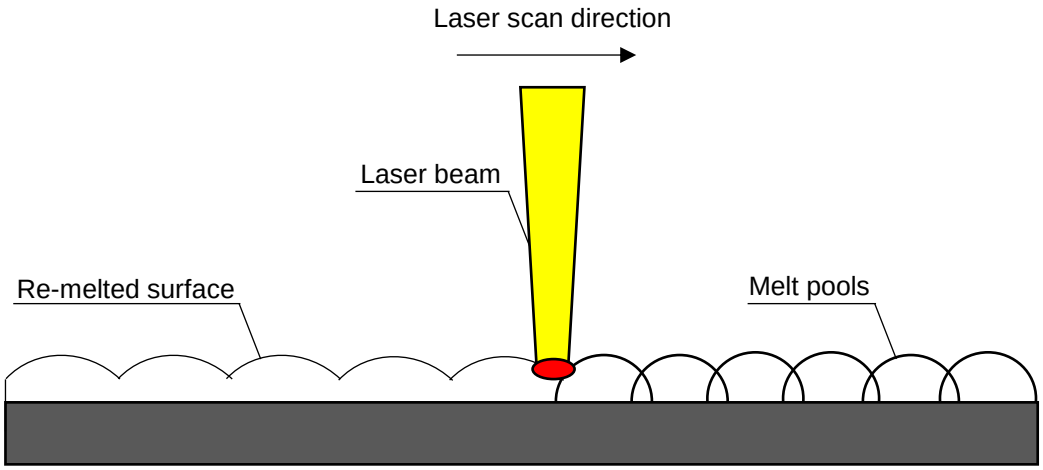

Fig. 2-6 - Schematic diagram of a re-melting laser scan in SLM

2.3 Research gap, hypothesis and questions

Evidently, selective laser melting is a significant new addition to processing metals from powder forms to finished components. Considering the freedom to fabricate more complex shapes relatively easily, the technology is considered as a viable alternative to traditional manufacturing in widely varying areas of application. However, the point-by-point and line-by-line consolidation often leads

to inappropriate coalescence between adjacent particles and layers, leading to porous cavities and cracking. Both material and process optimisation are attempted, together with optimum build orientations to mitigate the level of porosity. Laser re-melting is yet another approach employed to re- laser a layer, repair, and reduce the level of porosities and improve the physical and mechanical properties. Though positive results were reported with laser re-melting, the process conditions employed were quite limited in range. Considering the significant control, the re-melting of layers can offer both in terms of the material consolidation and also the possible heat treatment effects, it is important to revisit the process using the new developments in the technology. In particular, the higher power laser sources made available in the recent models of SLM systems have not yet been used to evaluate the possible effects of the laser re-melting approach.

The research gap identified thus is; possible roles of laser re-melting of individual layers on the mechanisms of material consolidation, physical and mechanical attributes have not been investigated yet using the higher ranges of power available with the modern systems for selective laser melting. Based on the trends reviewed from the current literature and with due consideration to the mechanism of material consolidation in SLM, the hypothesis proposed is:

Laser re-melting of each layer can be used as an effective means to control specific attributes of inter and intra layer consolidation in selective laser melting.

The research to be undertaken to prove this hypothesis raises the overarching research question:

What are the possible roles of re-melting each layer with varying process conditions on the mechanisms and mechanics of material consolidation in selective laser melting?

The research undertaken and presented in this thesis addresses this question by means of systematic experimental investigations designed and conducted applying selective laser melting. A specific grade of stainless steel is used as the base material for all the experimental investigations.

2.4 Methodology

2.4.1 Experimental materials and equipment

316L stainless steel, composition as presented in **Table 2-1**, is used to produce specimens for the re-melting experiments. It is an austenitic stainless steel with an extra-low carbon variation on the standard 316 alloy. The material is provided by Renishaw, the manufacturer of the selective laser melting equipment, in powder form with an average particle size of approximately 30 µm. A majority of the powder particles are spherical as shown in **Fig. 2-7**.

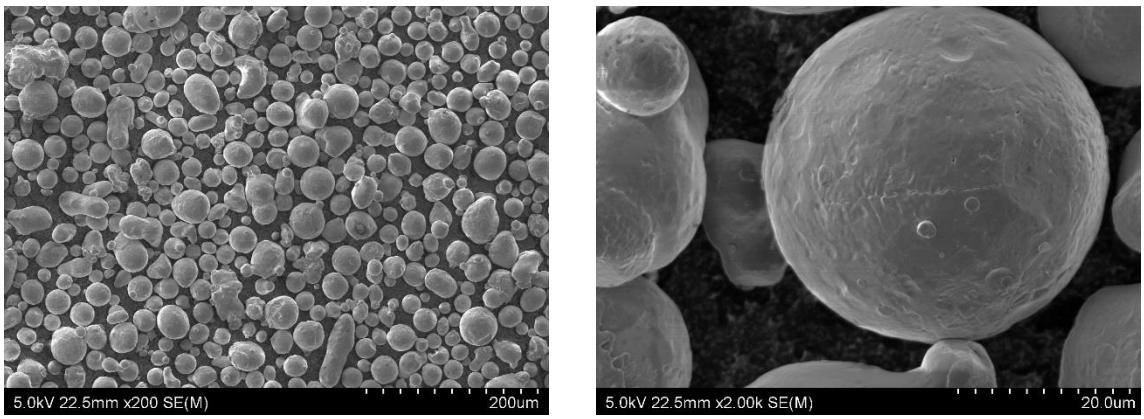

Fig. 2-7 - Particle morphology of the 316L stainless steel powder

Table 2-1 - Composition of the 316L stainless steel powder

Composition (w%)										
Cr	Ni	Mb	Mn	Si	N	O	P	C	S	Fe
16-18	10-14	2-3	<2	<1	<0.1	<0.1	<0.045	<0.03	<0.03	Balance

The selective laser melting equipment used is Renishaw AM250 (**Fig. 2-8**). The main characteristics of the system are the ytterbium-doped yttrium aluminium garnet (Yb:YAG) laser which has a wavelength of 1070 nm and a maximum laser power of 400 W; the argon atmosphere inside the build chamber in order to prevent contamination of powder from oxygen or nitrogen; the mild steel substrate plates that are maintained at 170 °C. Mechanical properties of 316L stainless steel parts when built with 200 W laser power with 50 μm layer thickness are presented in **Table 2-2**, according to Renishaw. It is evident that the mechanical properties between the melted layers, in the vertical direction, are generally much lower than along the horizontal directions. The horizontal surfaces, in which the laser was directly applied, obtained a more stable consolidation. On the other

hand, the interlayers have a greater variation of consolidation due to inconsistent contact with the heat source.

Table 2-2 - Mechanical property of 316L SLM parts (Renishaw)

Tensile strength (UTS)	Horizontal direction (xy)	662 ± 2 MPa
	Vertical direction (z)	574 ± 10 MPa
Hardness (Vickers)	Horizontal direction (xy)	212 ± 2 HV 0.5
	Vertical direction (z)	220 ± 6 HV 0.5
Surface roughness (Ra/Rz)	Horizontal direction (xy)	10 to 16 µm
	Vertical direction (z)	6 to 8 µm

Fig. 2-8 - Renishaw AM250

2.4.2 Experimental conditions

A laser beam spot size of 50 µm, a scan spacing of 0.14 mm and a layer thickness of 0.05 mm were applied in combination with the parameters in **Table 2-3** to build

cylindrical specimens. An appropriate range of energy density, from 110 J/mm^3 to 185 J/mm^3, was selected for SLM using AISI 316L stainless steel. The cylindrical specimens were produced with a continuous wave (CW) single-frequency mode Yb:YAG laser, with the build orientation as shown in **Fig. 2-9**. Three sets of samples are produced to study the effects of re-melting each layer in SLM. Set A is built with single pass laser scanning to represent the standard SLM characteristics; set B with double pass laser scanning while repeating with half of the original energy density; set C with double pass laser scanning while repeating with a quarter of the original energy density. The process parameters corresponding to sets A, B, and C, are shown in **Tables 2-4, 2-5**, and **2-6**, respectively. The energy densities are calculated using equation **Eq. 2-1** and numbered in ascending order. This is illustrated in **Fig. 2-10** where the sets and energy densities are labelled in red.

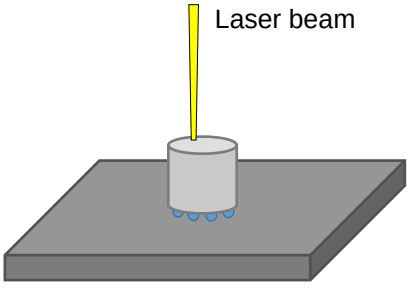

Fig. 2-9 - 316L stainless steel specimens build orientation

Table 2-3 - Selected range of ED for 316L SS specimens

	Speed (mm/s)	
Power (W)	**290**	**390**
300	**ED 3** = 148 J/mm^3	**ED 1** = 110 J/mm^3
375	**ED 4** = 185 J/mm^3	**ED 2** = 137 J/mm^3

Table 2-4 - Set A parameters

	Power (W)	Speed (mm/s)	ED (J/mm^3)
A1	300	390	110
A2	375	390	137
A3	300	290	148
A4	375	290	185

Table 2-5 - Set B parameters

	First scan	Second scan		
	Same as	**Power (W)**	**Speed (mm/s)**	**ED (J/mm^3)**
B1	A1	150	390	55
B2	A2	187.5	390	69
B3	A3	150	290	74
B4	A4	187.5	290	92

Table 2-6 - Set C parameters

	First scan	Second scan		
	Same as	**Power (W)**	**Speed (mm/s)**	**ED (J/mm^3)**
C1	A1	75	390	27
C2	A2	94	390	34
C3	A3	75	290	37
C4	A4	94	290	46

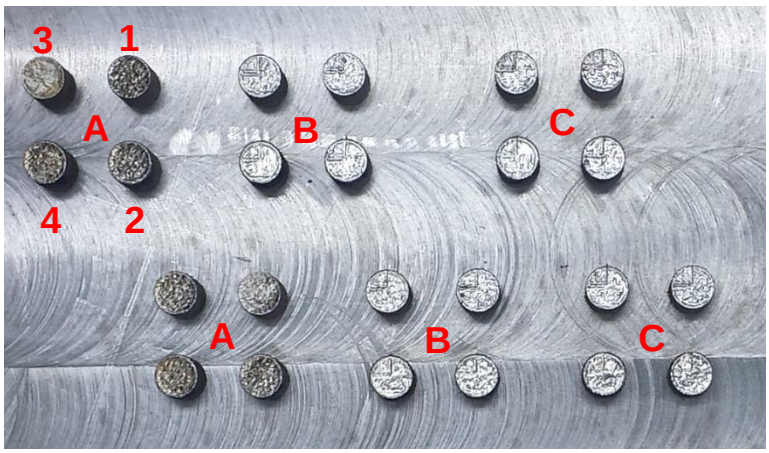

Fig. 2-10 - 316L stainless steel build design

2.4.3 Metallography

Light optical microscope (LOM) and scanning electron microscope (SEM) images are used for microstructural analyses of the effects of re-melting on SLM 316L stainless steel. The cylindrical samples are wire-cut in half, across the diameter, using EDM. In order to study the revealed cross-sectional area, the specimens are hot mounted with the Struers mounting press system (**Fig. 2-11**) using 23 mL of PolyFast, a thermosetting resin with carbon filler, into 30 mm diameter samples. The 6 minutes of heating cycle is applied at a temperature of 180°C with a force of 20 kN, then water-cooled for 3 minutes at a high cooling rate.

A Buehler MetaServ twin rotary grinder (**Fig. 2-12**) is used for a four-step grinding process using Stuers waterproof silicon carbide papers in the order of 180, 500, 1200 and 2400 grit sizes. Polishing is achieved using a Struers LaboPol-2 polishing machine (**Fig. 2-13**) in two steps at 500 rpm. With corresponding polishing pads, diamond polishing (DP-paste) paste with 6µm and 1µm monocrystalline diamonds are used.

Fig. 2-11 - Struers mounting press

Fig. 2-12 – MetaServ twin rotary grinder

Fig. 2-13 - Struers polishing machine

The final process before observing the specimens under the microscope is etching. In attempts of identifying the appropriate chemical reagent for 316L stainless steel, a variety of etchants are trialled: Marble's reagent (10 g $CuSO_4$, 50 mL HCl, and 50 mL H_2O) for up to 10 seconds, dilute aqua regia (15 mL HCl, 5 mL HNO_3, 100 mL H_2O), and Beraha's reagent (100 mL H_2O, 20 mL HCl, and 1 g $K_2S_2O_2$) for up to 120 seconds. After the initial trials, aqua regia (75 mL HCl, 25 mL HNO_3, and 100 mL H_2O) is used to immerse the freshly polished samples for 40 seconds and the reaction was visible to the eye as shown in **Fig. 2-14**.

Light optical photomicrographs and SEM images are taken immediately after the etching process for the best results. Prior to inserting in the SEM, the samples are cleaned using an Elma S10H Elmasonic ultrasonic cleaner with a frequency of 37 kHz. The ultra-high resolution analytical field-emission SEM Hitachi SU-70 shown in **Fig. 2-15** is used for all SEM imaging.

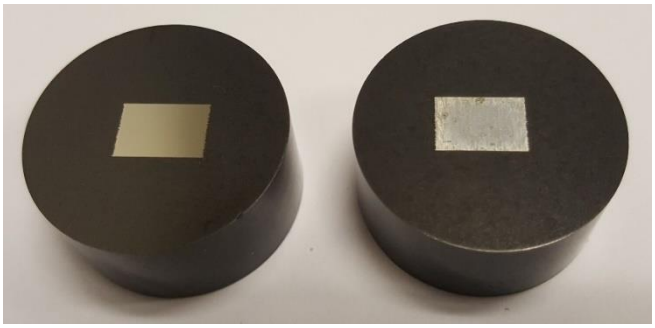

Fig. 2-14 - SLM 316L stainless steel specimens, before and after etching

Fig. 2-15 - Hitachi SEM system

2.4.4 Tensile testing

For tensile testing, three sets of rectangular specimens are built using the conditions as presented in **Table 2-7**. The re-melted specimens, sets 2 and 3, are built using the same parameters as set 1, with no re-melting, then the second scans with corresponding laser parameters according to **Table 2-7**. Each set of samples are varied in the build orientation longitudinally: set A - 0° / horizontal, set B - 45° / diagonal and set C - 90° / vertical. The meander laser scanning strategy is applied for all the tensile test specimen builds, with which the scanning direction of the laser beam alternates by 90° for every layer as illustrated in **Fig. 2-16**.

Table 2-7 - Build parameters for tensile testing

	First scan	Second scan		
	Power (W)	**Power (W)**	**Speed (mm/s)**	**ED (J/mm^3)**
1	375	-	383	140
2	375	200	1300	140, 22
3	375	100	1300	140, 11

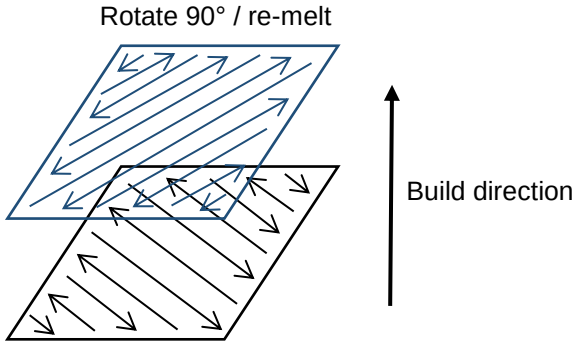

Fig. 2-16 - The meander laser scan strategy

The rectangular specimens are wire-cut using electrical discharge machining (EDM) into the geometry of the dog bone shapes according to the ASTM standard E8 / E8m – 09 (**Fig. 2-17**), in order to control the failure location. The dog bone specimens are then loaded onto a Tinius Olsen H50K-S UTM benchtop materials tester with a 50 kN capacity equipped with an extensometer (**Fig. 2-18**). The tensile test speed is set to 3 mm/min and the tests are performed at room temperature.

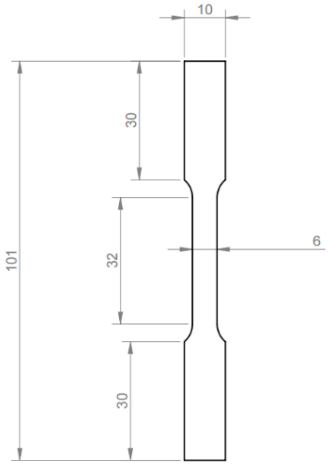

Fig. 2-17 – Dog bone specimens according to ASTM standard E8/E8m - 09

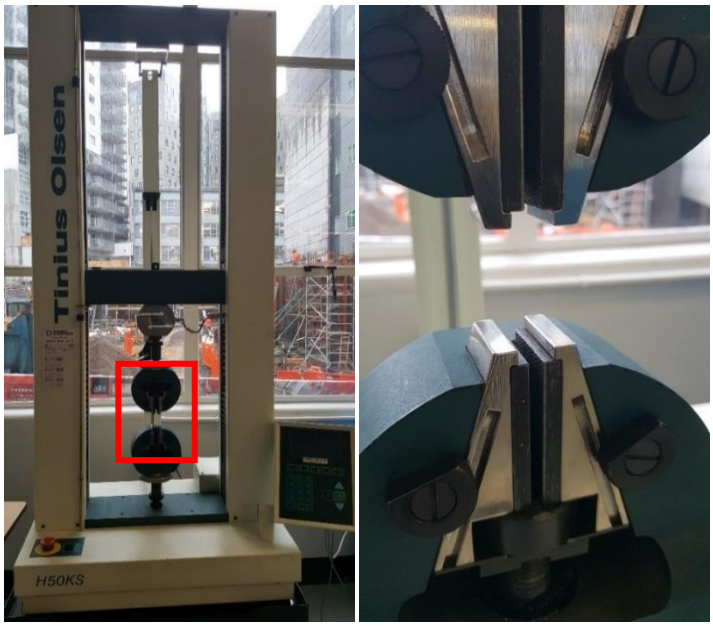

Fig. 2-18 - Tinius Olsen tensile tester

2.4.5 Hardness

The hardness values of the SLM 316L stainless steel samples are measured using Rockwell hardness C (HRC). This testing device, shown in **Fig. 2-19**, uses a spheroconical diamond pointer to create an indent in the material using a minimum load of 10 kg / 98 N and a maximum load of 140 kg / 1373 N. The hardness tests are conducted based on the top surfaces of the cylindrical specimens printed. The bottom surfaces are neglected from these trials as they are attached to the substrate plate during the build and therefore damaged during the removal process. The lateral surfaces of the cylindrical samples are also neglected as the hardness values parallel to the build direction are inconsistent.

Fig. 2-19 - Rockwell Hardness C testing

2.4.6 Porosity

The amount of porosity in each specimen was determined by using the following equation:

$$Porosity = \frac{M_{th} - M_a}{M_{th}} \times 100\ [\%] \quad \text{.....Eq. 2-2}$$

where M_{th} is the theoretical mass and M_a is the actual mass.

The theoretical mass is calculated using the volume obtained from the dimensions of each samples, height and diameter of the cylinder, which is multiplied by the density of 316L stainless steel powder material, 7.99 g/cm^3, as provided by Renishaw. The actual mass is measured using a mass balance with an accuracy up to ±0.0001 g.

2.4.7 Surface roughness

The lateral surface roughness of the cylindrical SLM 316L stainless steel specimens are measured using a Taylor Hobson Form Talysurf 50 surface profilometer system as shown in **Fig. 2-20**. Each specimen is placed on a flat surface and clamped securely. The testing length is set to 6 mm, just under the average height of the samples which is 7.04 mm. Three surface roughness values are recorded: arithmetic average (R_a), root mean squared (R_q) and ten-point mean roughness (R_z) with five peaks and five valleys. Surface profile graphs are also generated for each trial.

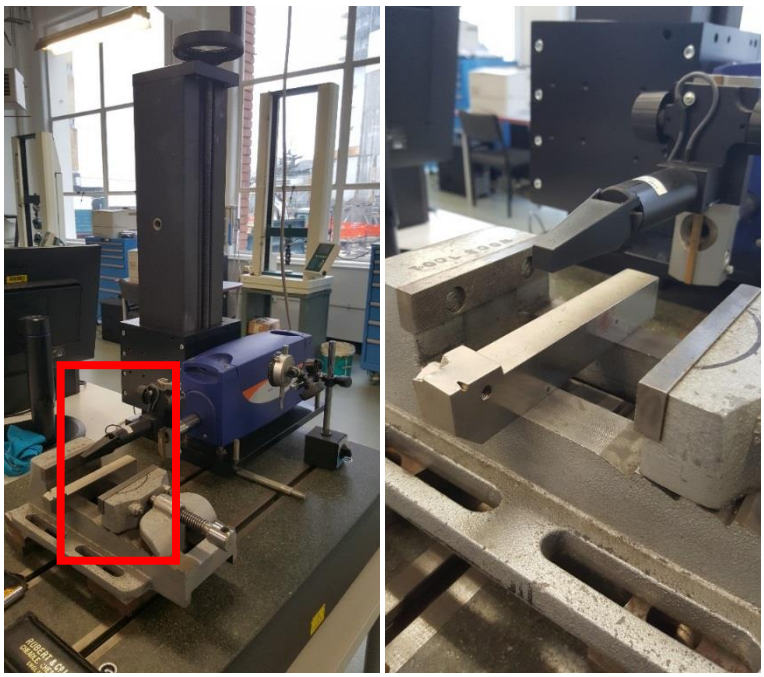

Fig. 2-20 - Taylor Hobson Precision surface roughness testing

Chapter 3

Mechanism of Consolidation with Laser Re-melting

3.1 Process-structure relationships

The study of metallography is crucial in additive manufacturing as the heat transfer mechanism is different to traditional manufacturing methods such as casting. The complex heat transfer in selective laser melting is produced by concentrated laser heat source scanning a powder bed which irradiates metal powders, forming melt pools. The melted scan tracks will undergo rapid cooling in the direction parallel to the build direction, creating non-equilibrium solidification. This involves grain refinement and possible limitations on solid solubility. With selective laser re-melting, the solidified melt pools are either fully or partially re-melted depending on the energy density settings. This further refines the grain structure due to the large temperature gradient.

The mechanisms of powder consolidation and the subsequent microstructures change from the normal SLM to the selective laser re-melting situations. These differences are observed here based on both optical and scanning electron photomicrography. The process-structure relationships will be established based on the metallographic characterisation. These relationships will be integrated with the process property relationships later in order complete the understanding of the overall cycle of changes with the laser re-melting approaches.

3.2 Light optical microscopy

Photomicrography based on light optical microscopy is used to observe both the macro and micro structural variations. The differences in the formation of melt pools and melt pool borders on the cross-sections of the 316L stainless steel specimens with and without re-melting are noted. The melt pools are formed as elongated semi-circular troughs indicating successful fusion of melted and solidified zones during the build of the SLM part. The height of the troughs, the maximum distance between the top and the bottom borders of each melt pool, vary from approximately 30 µm to 80 µm for single scan samples and approximately 30 µm to 100 µm in double scan samples. These are dependent on parameters such as laser spot size, power, and scan speed. The double scan samples have bigger troughs, in terms of both height and width, as the re-melting scans consolidate adjacent melt pool areas to form larger troughs or elongated layers.

The trough-like solid formations resulting from multiple passes of the laser beam in the single-pass cases as presented in **Fig. 3-1** show the varying heights and widths of different solid formation zones. They are relatively similar across the different energy densities but show some variation within each energy density. The solid fronts from different melt pools do not mix completely and leave out traces of scan tracks while the solid formation within each melt pool could have resulted from the crystal structure growth within the melt pool. The distinct curved lines represent the cross-sectional views of different scan tracks. The laser scan tracks indicate lack of fusion and discontinuities in the material consolidation. The scan tracks also suggest to be sources of segregation of impurities and

intermetallic compounds. The number of multiple closed spaced solid fronts increase moderately with increasing energy density. At some places the solid front lines are missing probably due to significant inter-strand mixing and consolidation of the liquid metal.

In the case of samples with laser re-melting, there is evidence of the elimination of the melt pool borders due to re-heating as shown in **Fig. 3-2 a)** and **Fig. 3-3 a)**. This causes the layers of melt pool troughs to become either elongated or enlarged, where the former can be seen in the re-melted samples with half energy density repetition while the latter is prominent in the re-melted samples with quarter repetition. The higher magnification photomicrographs of **Fig. 3-2** illustrate the formation of the horizontal continuous inter-border layers as a result of consolidation of adjacent melt pools during the secondary laser scans. This is most comparable to a lamellar structure which is desired in SLM parts for better mechanical properties. Similarly, the higher magnification photomicrographs of **Fig. 3-3** show melt pools with deeper troughs where the shapes and the structure are still comparable to those of samples with single scanning at higher energy density.

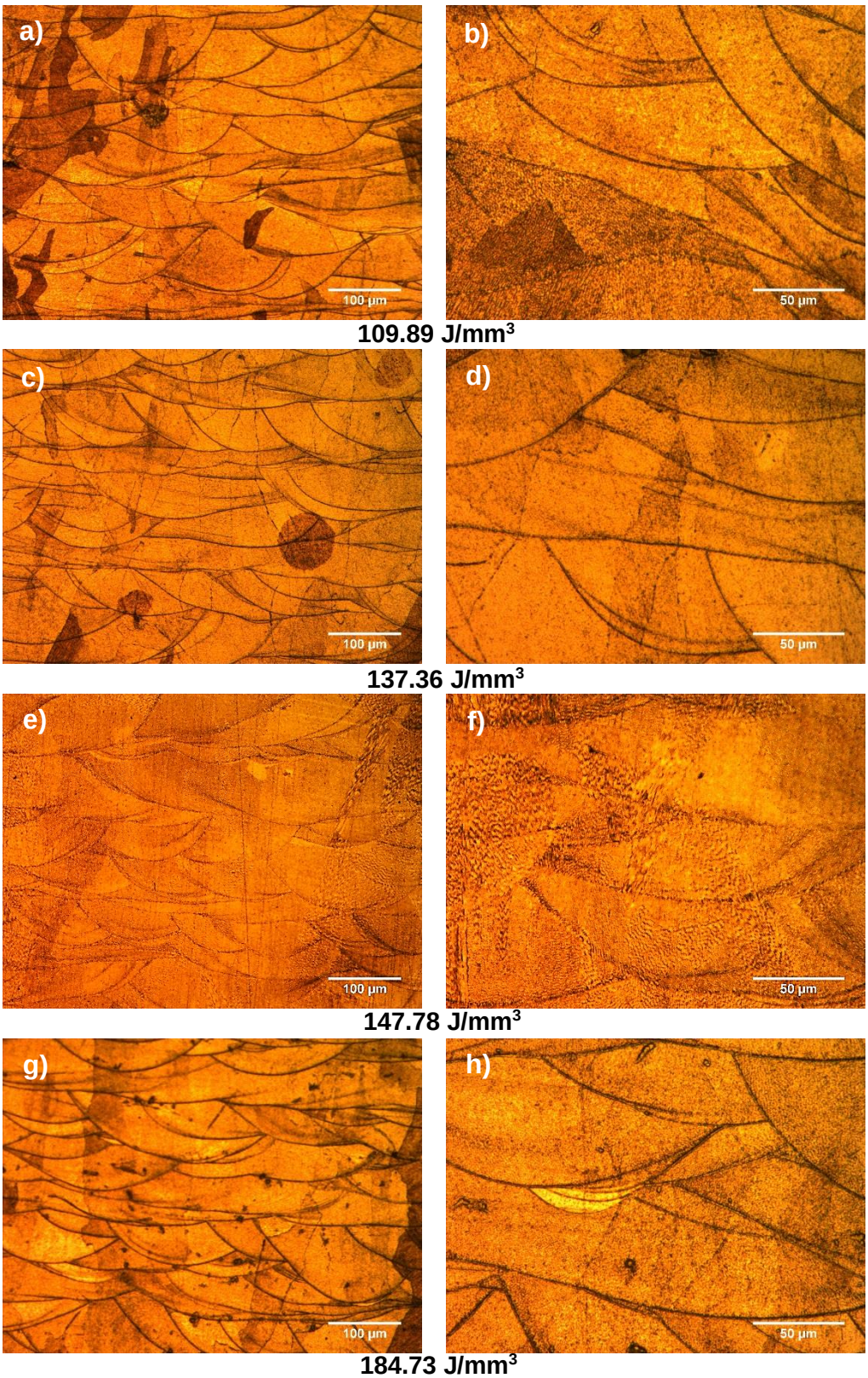

Fig. 3-1 – Photomicrographs of cross-sections of samples with single pass laser melting

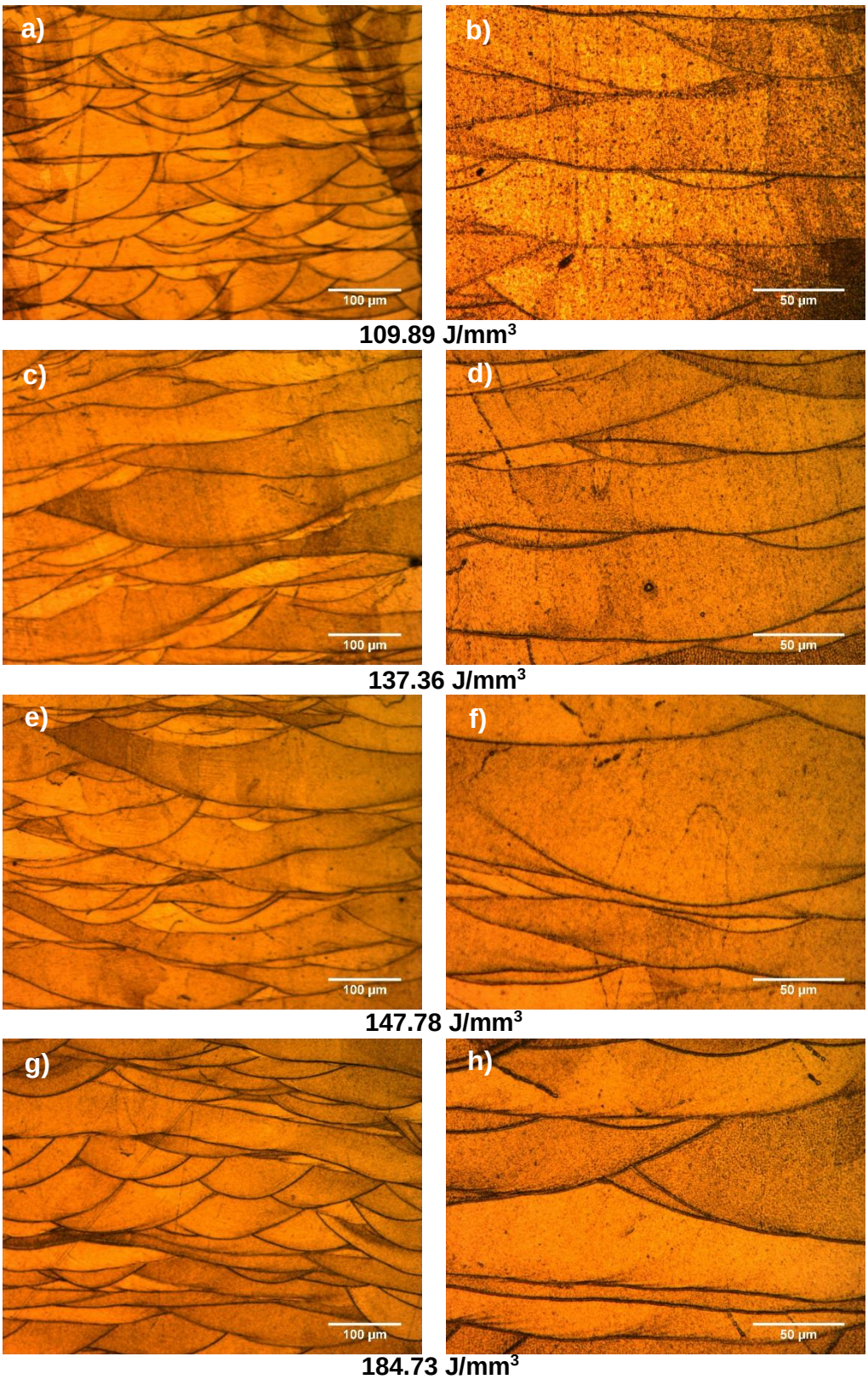

Fig. 3-2 - Photomicrographs of cross-sections of samples with double pass laser re-melting half ED repetition

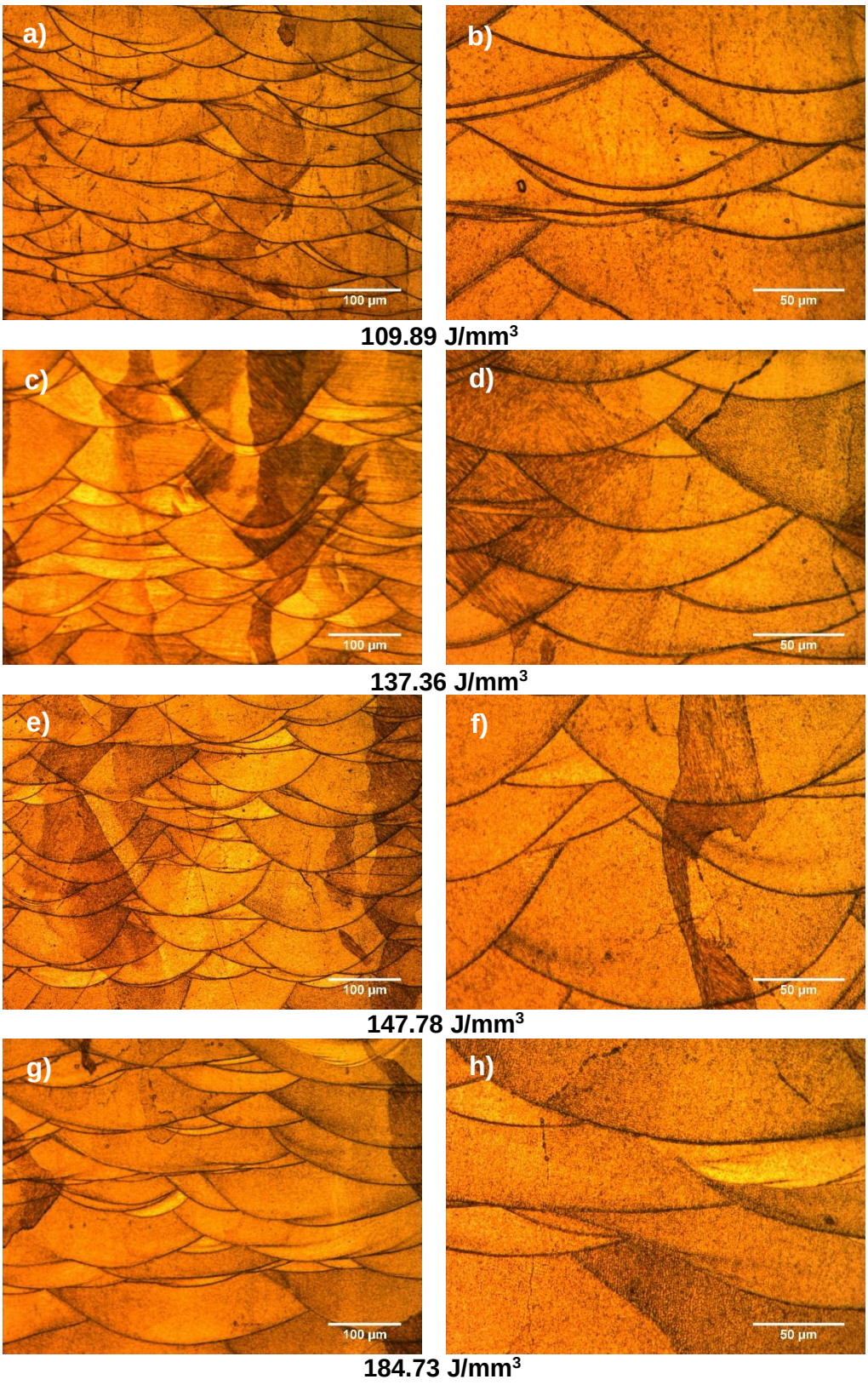

Fig. 3-3 - Photomicrographs of cross-sections of samples with double pass laser re-melting quarter ED repetition

3.3 Scanning electron microscopy

Microstructural study of a material is a vital part of a complete parametric analysis as it should correspond to the physical properties. For the purpose of this study, the critical areas of the microstructures are shown on a cross-sectional SEM image of a 316L stainless steel sample produced by SLM. The melt pools are divided by thin, white lines labelled as melt pool borders that are also observed in the optical photomicrographs presented earlier. The pores generally appear along the melt pool borders or have a spherical shape, or occasionally as elongated cracks as identified in **Fig. 3-4** below.

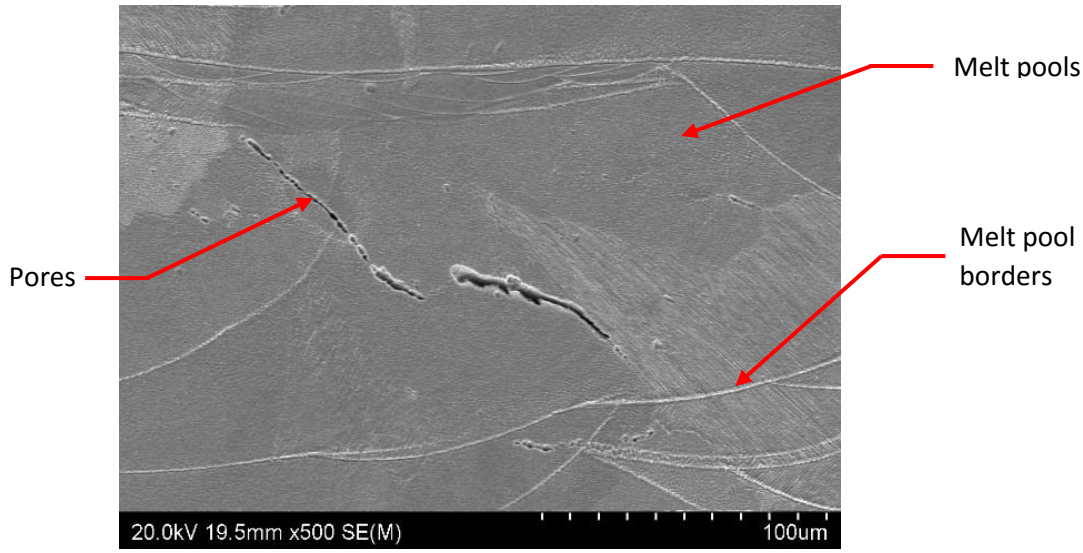

Fig. 3-4 - Critical areas of the microstructures

The overall structures of the melt pool boundaries are seen in the same patterns as earlier, as may be observed from the photomicrographs of **Fig. 3-5 (i)** and **3-6 (i)**. Micro-level observation at higher magnifications reveal intragranular cellular segregation network (ICSN) structures inside the columnar grains as shown in **Fig. 3-5 (ii),** and **3-6 (ii)**. This intragranular cellular segregation network structure

cannot be defined as grains as it shares similar crystallographic orientation as the adjacent cells. These structures appear equiaxed or elongated depending on the growth direction of the columnar grains containing them as reported by Zhong *et al.* [50]. The equiaxed structures are generally angular, not quite spherical, but consist of fairly equal sides defining their perimeters. They appear in the transverse direction while the elongated structures in the longitudinal direction mirror the columnar grains. This variation in solidification structure can occur within one melt pool and the effect of solute and thermal gradients on this is defined by the following equations:

$\frac{G_L}{R} < \frac{\Delta T}{D_L}$ For plane equiaxed solidification ***……Eq. 3-1***

$\frac{G_L}{R} > \frac{\Delta T}{D_L}$ For cellular and columnar solidification ***……Eq. 3-2***

where G_L is laser melting temperature gradient, R is growth rate, ΔT is solidification undercooling and D_L is the diffusion coefficient [51].

The ratio of G_L over R represents the stability of the solidification microstructure, and hence the final structure, while the cooling rate in terms of the product of G_L and R determines the fineness of the structure. This is also evident in laser surface re-melting studies, where the formation of homogeneous cellular structures or cellular dendritic structures were found due to rapid solidification [20]. Microstructures at a higher magnification (**Fig. 3-5 (ii)** and **Fig. 3-6 (ii)**) show that these cells are largely separated by melt pool borders but are able to form within the same melt pool.

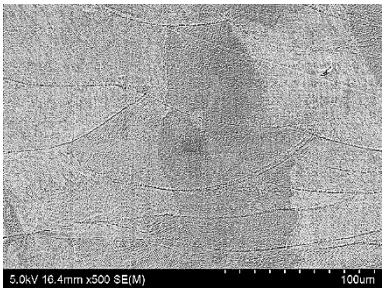

a) Single pass

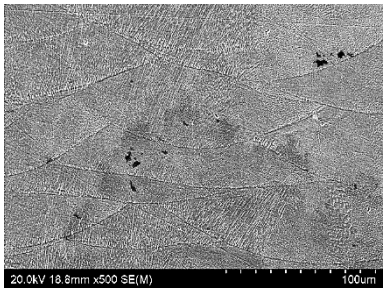

b) Double pass at half ED

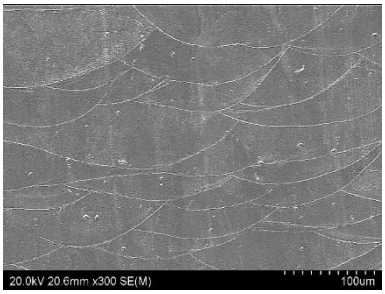

c) Double pass at quarter ED

i) Melt pool borders

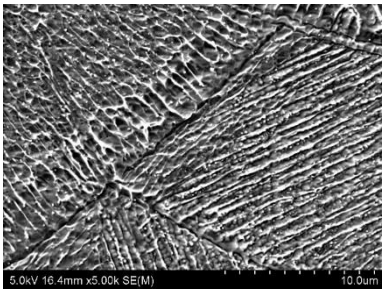

a) Single pass

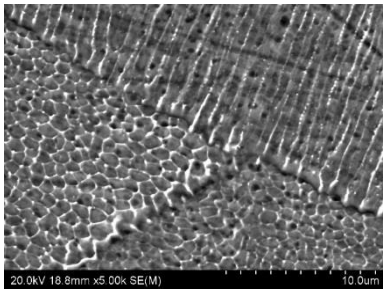

b) Double pass at half ED

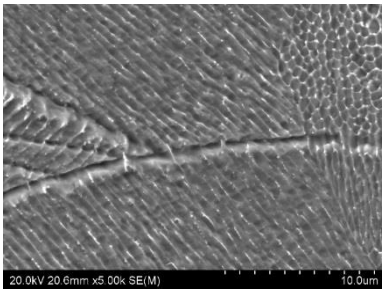

c) Double pass at quarter ED

ii) Cellular structures

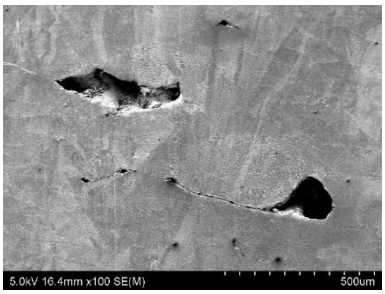

a) Single pass

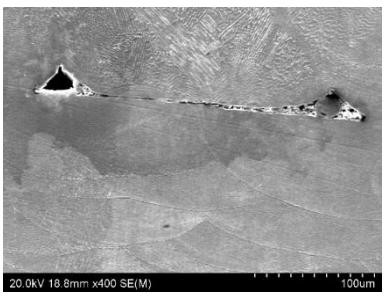

b) Double pass at half ED

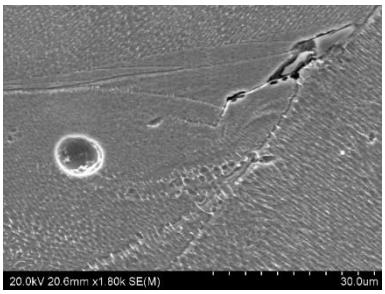

c) Double pass at quarter ED

iii) Porosity

Fig. 3-5 - SEM photomicrographs of microstructures obtained with at 109.89 J/mm^3

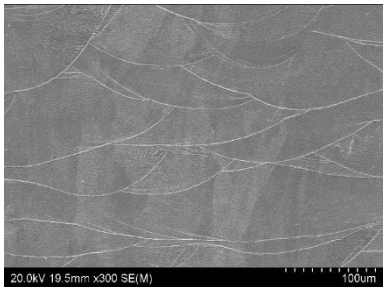

a) Single pass

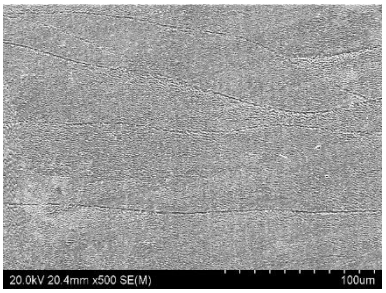

b) Double pass at half ED

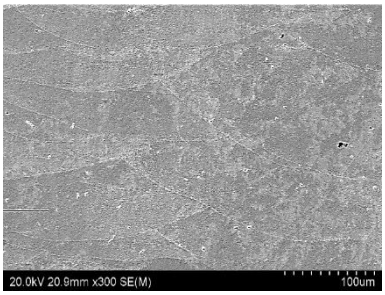

c) Double pass at quarter ED

i) Melt pool borders

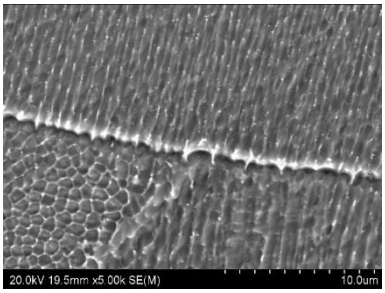

a) Single pass

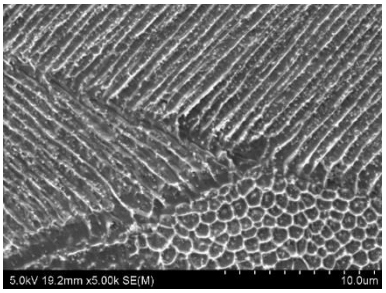

b) *Double pass at half ED*

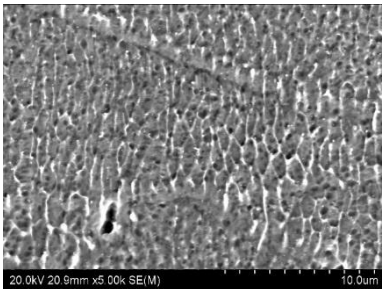

c) Double pass at quarter ED

ii) Cellular structures

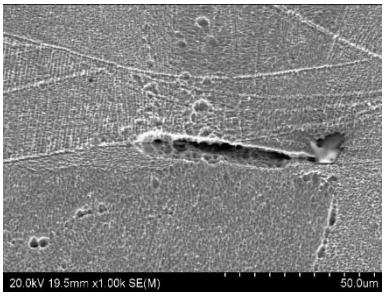

a) Single pass

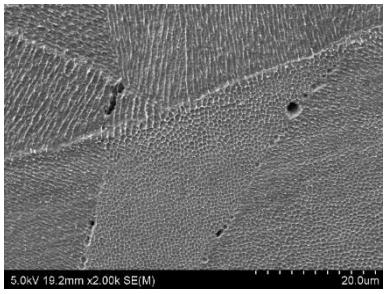

b) Double pass at half ED

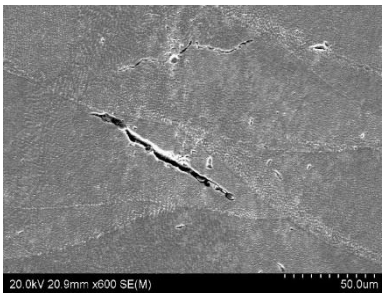

c) Double pass at quarter ED

iii) Porosity

Fig. 3-6 - SEM photomicrographs of microstructures obtained with at 184.73 J/mm^3

The aforementioned G_L and R ratio could be the explanation behind the occurrence of the intragranular cellular segregation network structure in SLM parts. With extremely large temperature gradients in the SLM process, a high G_L and R ratio, the growth of cellular dendrites dominate over planar front growth [50]. This is also in relations to compositional fluctuations and constitutional supercooling / undercooling of conventional casting, which is also a rapid solidification process [52]. The compositional fluctuations are due to the "slow kinetics of homogeneous alloying of large atoms of heavier elements" [53], consequently forming the intragranular cellular segregation network structure. However, the precise forming mechanism of the intragranular cellular segregation network structure is yet to be studied as the SLM process produces parts with various rapid melting, cooling and solidification conditions. With G_L up to 10^7 K/s, where the formation of columnar structure is favoured over dendrites, that vary depending on the material property, part geometry, gas flow rate and laser parameter [54], the microstructures found in SLM parts are contradistinctive to those found in traditionally manufactured parts.

Comparing the single pass and the double pass with half energy density cases at both energy densities, the cellular structures appear to be strikingly similar. This is probably due to the re-melting at relatively higher energy density levels, leading to recrystallisation and the formation of fresh cellular structures that are similar to the original cellular structures. On the other hand, the cellular structures in both cases at the quarter energy density repetition (**Fig. 3-5 (i)c)** and **Fig. 3-6 (ii)c)**) are different from the other two cases, in that the cells seem to be camouflaged and stretched across the grain boundaries. This could be possibly due to the

initiation of recrystallisation but incomplete transformation due to the lower repeated energy density levels.

Considering the single pass laser scanning sample with energy density of 184.73 J/mm^3 (**Fig. 3-6 (ii)a)**) consists of columnar cells that shows growth in the vertical direction, parallel to the build direction. However, not all columnar grains follow this trend; instead, they display grain growth in the direction perpendicular to the melt pool border that they stemmed from due to various heat flux directions. This is best illustrated in the double pass case at half energy density samples in **Fig. 3-5 (ii)b)** and **Fig. 3-6 (ii)b)**. Furthermore, the single scan sample with energy density at 109.89 J/mm^3 (**Fig. 3-5 (ii)a)**) shows that the columnar grains began growing from one end to the other of a melt pool. This suggests that the direction of the grain growth during solidification is dependent on the laser scanning strategy, hence the temperature gradient. This was consistent with the results reported by Zhong *et al.* [50].

There are several equiaxed cells that appear in zones where three melt pools are in contact, such as in **Fig. 3-6 (ii)a**. This is possibly caused in single laser pass samples during recrystallization where these zones undergo higher temperatures than borders with two adjoining melt pools or within a melt pool. On the other hand, double pass laser scanning with half energy density repetition samples consist predominantly of equiaxed cells with evidence of grain growth across the melt pool borders. The double pass with quarter energy density repetition samples showed mixed characteristics of both single pass and double pass with half energy density repetition samples as expected. The microstructure shows a combination of both equiaxed and columnar grain growth that appear across melt

pool boundaries. A closer observation of the cross-section displays equiaxed cells of different sizes where there are sizes comparable to that of the single pass samples and smaller, refined cells. These grain growths have occurred at zones connecting three melt pools, whereas the larger equiaxed cells are visibly concentrated along melt pool borders.

Defects and imperfections are also common in SLM metal parts [33, [40]. Comparing the photomicrographs of **Fig. 3-5 (iii)** and **Fig. 3-6 (iii)**, it may be noted that lack-of-fusion defects occurred predominantly at the grain boundaries. In the case of the single scan samples at both energy densities, these defects are quite large and spherical at some places while they are also stretched along the grain boundaries in other cases. Evidently, the laser re-melted cases at both levels and with both energy density settings appear to have reduced the level of the defects to varying degrees. It is likely that the repeated heating allowed either liquid or solid state sintering to take place and seal off some of the existing porous cavities. This will be further established when the porosity results are evaluated in the next chapter.

Non-equilibrium solidification occurs in SLM where epitaxial growth in metal parts are commonly found due to various heat fluxes caused by the concentrated laser melting and fast cooling similar to the welding processes. Large epitaxial growth was observed in all SLM 316L stainless steel samples, as shown in **Fig. 3-7**. Across all scan strategies, single and double scanning, and energy density settings, epitaxial growth extends vertically through multiple melt pools. It is evident that the severe temperature gradients caused by rapid cooling rates and large degree of undercooling, as discussed previously for SLM caused the grains

to follow the direction in which the temperature gradient was at its maximum. Epitaxial solidification is commonly found in SLM 316L stainless steel.

Evidently, epitaxial growth is more pronounced in double pass laser scanning samples. As already noted from **Fig. 3-5 (ii),** and **3-6 (ii)** the sub-grain intragranular cellular segregation network microstructures show that they grow across the fusion zones between melt pools in re-melted samples depending on the level of the repeated energy density, whereas the single scan samples retain distinct melt pool borders. This suggests that the re-melting scans may cause an increase in the temperature gradient, allowing the grains to continue growing through the solidified substrate layers, extending onto the next layer. This is an ideal characteristic in SLM parts as a reduction in fusion zones lead to an increase in density and mechanical properties such as tensile strength.

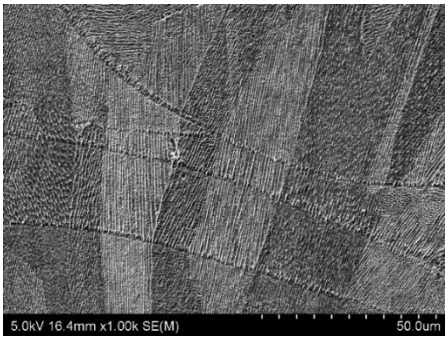

a) Single pass, 109.89 J/mm³

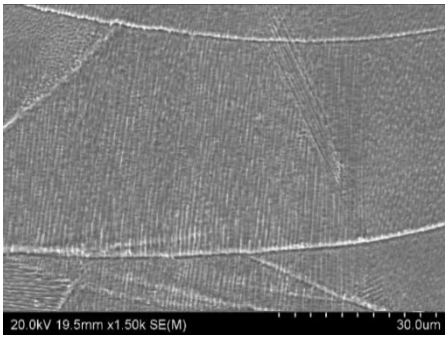

b) Single pass, 184.73 J/mm³

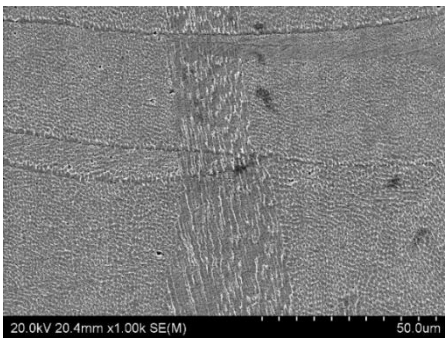

c) Double pass half ED repetition, 184.73 J/mm³

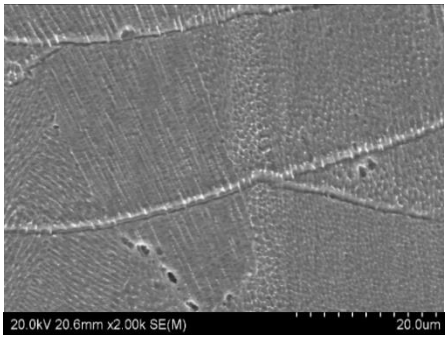

d) Double pass quarter ED repetition, 109.89 J/mm³

Fig. 3-7 - SEM images showing epitaxial growth in SLM 316L stainless steel

Chapter 4
Mechanical and Physical Characteristics

4.1 Further characterisation of laser re-melting

Selective laser melting process parameters have significant impacts on the mechanical and physical characteristics of AISI 316L stainless steel parts due to the possible changes in the melting and solidification mechanisms of the powder materials. Varying energy density settings produce different results in the consolidation of each layer which consists of multiple laser scan tracks. Furthermore, the re-melting process in selective laser re-melting with additional energy density settings enable changes to the already formed melt pools.

Parametric analysis involving mechanical and physical characteristics of selective laser re-melted parts is crucial as the build process consists of several confounding stages; the quality of a single laser scan track will affect the next, while the quality of a layer which consists of multiple single laser scan tracks will affect the next and so on. Better physical and mechanical properties may be obtained with proper section of the re-melting parameters. Though laser re-melting increases the overall production time, the ability to overcome some of the inherent shortcomings of the process make it significant and useful eventually.

4.2 Percent elongation and tensile strength

The dog bone 316L stainless steel specimens shown in **Fig. 4-1** and built at three different orientations are subjected to tensile testing. The appearance of the top surfaces of these samples are similar to the surface qualities of cylindrical samples which will be discussed in Section 4.5. The sample built at 0°, where the top surface is parallel to the substrate plate and perpendicular to the build direction, has the shiniest surface. Evidently, the sample built at 45° has a rougher surface with more texture and the sample built at 90° has the dullest surface.

Fig. 4-1 - Tensile testing specimens (from top to bottom: 90°, 45°, 0°)

Results of the tensile tests conducted as per the conditions listed in **Table 2-7** of Chapter 2.4.4 are presented in **Table 4-1**. It may be recalled that the 1, 2, and 3 numbers in the first column refer to the cases single and double scan strategies at varying energy density levels. The elongation at failure is represented in percentage using the equation:

$$Elongation = \frac{Elongation\ at\ failure}{Initial\ gauge\ length} \times 100 \ \ [\%] \qquad \textbf{.....Eq. 4-1}$$

where the initial gauge length is given in **Fig. 2-17**.

The ultimate tensile strength is calculated using the equation:

$$UTS = \frac{Load\ at\ failure}{Initial\ gauge\ area} \ \ [\text{MPa}] \qquad \textbf{.....Eq. 4-2}$$

where the load at failure is measured in kN and the cross sectional area of the gauge in the dog bone, in m, was taken before the testing.

It is clearly evident from the data of **Table 4.1** that the samples produced at 45° orientation scored the best in terms of the percent elongation in all the three cases. The 0° cases scored the least in terms of the percent elongation. Another consistent observation that may be made is that in most cases, the percent elongation reduced, though slightly, from the single scan to the double scan at quarter energy case via the double scan at half energy setting. Possibly, the laser re-heating led to a possible heat treatment resulting in a loss of the ductility of the material. The loss of ductility with the 0° case is mostly due to the directional nature of the material structures resulting from the laser scan strategies as against the horizontal orientation of the specimen. Both 45° and 90° orientations perhaps resulted in the best formation mechanism of the layers and the inter layer bonding leading to the better ductility values.

Table 4-1 - Elongation and ultimate tensile strength of SLM 316L stainless steel

		Elongation (%)	UTS (MPa)
1	0°	26.49	604.88
	45°	38.57	551.59
	90°	35.92	554.79
2	0°	17.00	594.23
	45°	35.82	560.61
	90°	32.97	592.16
3	0°	15.78	592.96
	45°	39.02	570.98
	90°	28.82	580.86

The tensile strength results are illustrated as bar charts in **Fig. 4-2** for better clarity. It is clearly evident that the 0˚ cases in all three different settings resulted in the higher tensile strengths. This is due to the directional alignment of the growth of the internal structures with the loading direction. The 45˚ cases scored the least in terms of the tensile strength results, as against the improvement achieved in the ductility levels. It may be due to the stair-case effects leading to the stress concentration and lack of strength in the longitudinal direction.

The 90˚ orientation in many cases is a compromise between the two and is mainly due to the relatively weak inter-layer coalescence due to the small cross sectional areas on which the laser is acting. However, striking differences can be noticed in the results with the 90˚ cases with the laser re-melting approaches from the second and the third sets of bar graphs in **Fig. 4-2**. This is mainly due to the

improvements achieved in the inter-layer bonding from the repeated laser interactions at different energy levels. This effect of laser re-melting is better at the higher energy density settings as is the case with the middle set as the repair and rehabilitation of the layers and the inter layer zones appear to be more dominant with smaller sintering areas. Overall, it may be noticed that the laser re-melting approach is more effective in thin sections in terms of improving the tensile strength.

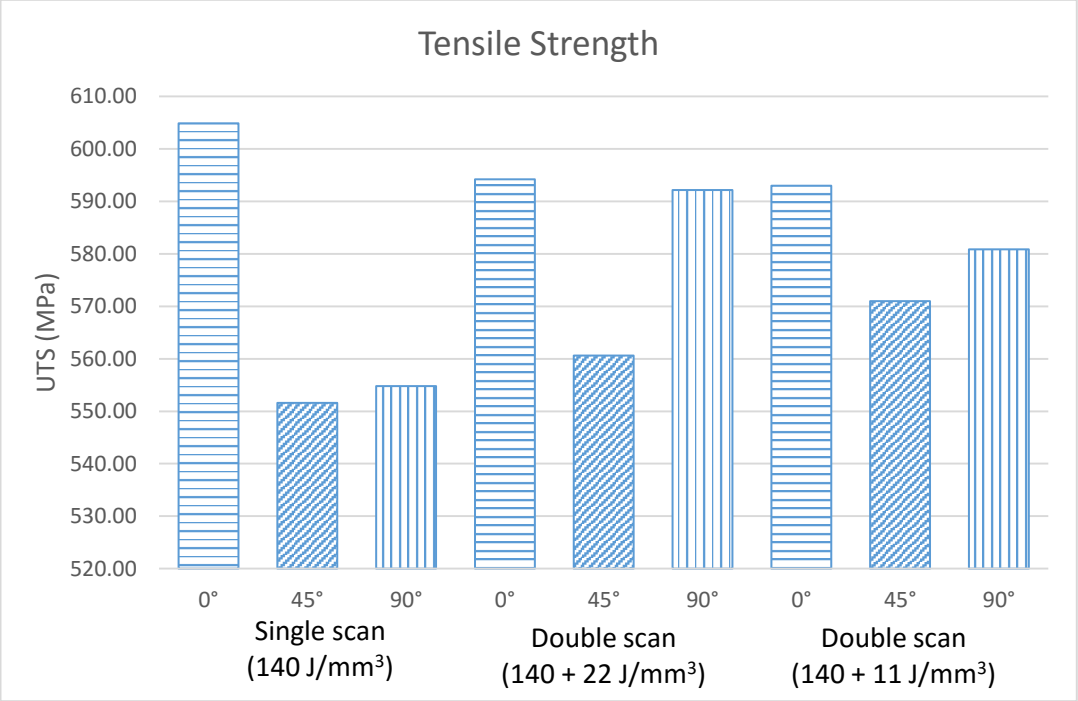

Fig. 4-2 - Tensile strength of SLM 316L stainless steel specimens

4.3 Hardness

Results of the hardness tests conducted on the top surfaces of the cylindrical 316L samples printed by selective laser melting with varying conditions are

presented in **Fig. 4-3**. Hardness tests on each specimen are repeated four times and the average values together with the error bars are presented in **Fig. 4-3**. It may be noted that the experimental variations are quite high due to variations within the samples. Considering the overall trends in the average values and the large error bars, it may be noted that the variation in the hardness values is not significantly high from one set of conditions to the other. However, the lowest energy density at 300 W and 390 mm/s proved to be the ideal setting for single scanning as it resulted in better hardness over the re-melting cases.

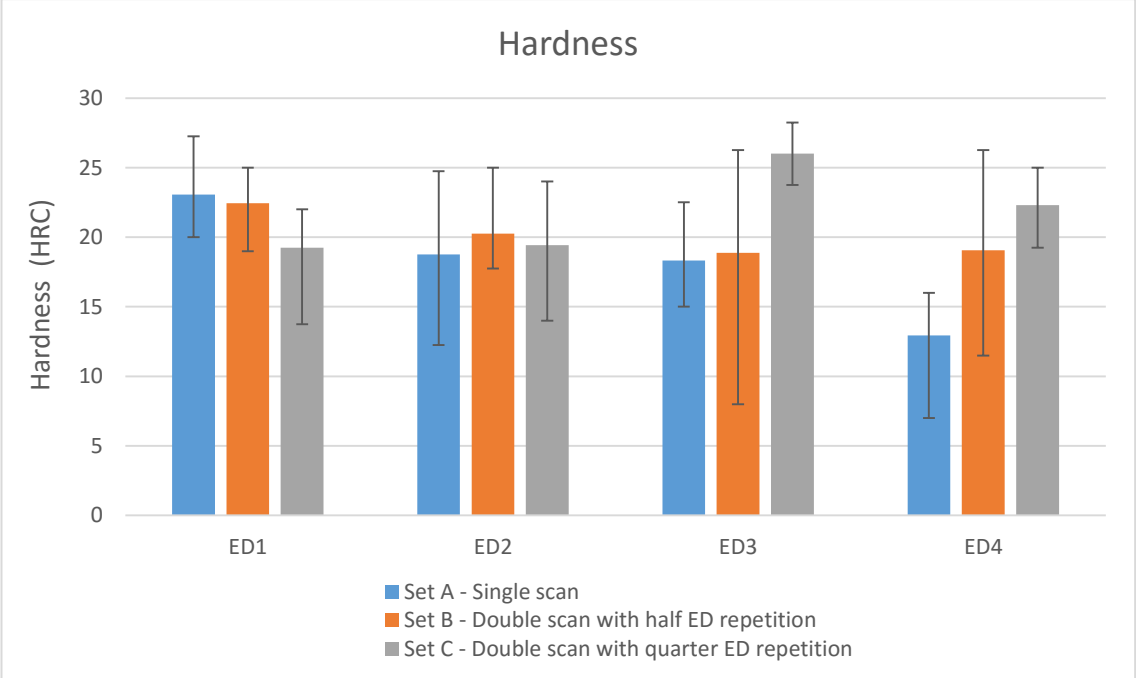

Fig. 4-3 – Hardness of SLM 316L stainless steel specimens

Out of the re-melted samples, the double scan with half energy density repetition had greater hardness than quarter energy density repetition in the lower energy density settings and vice-a-versa at higher energy density settings. The double scan with half energy density repetition specimens decreased slightly with increasing energy density, while the double scan with quarter energy density

repetition specimens, on the other hand, increased overall, producing the highest hardness values at energy density of 147.78 J/mm^3.

Both single scan and double scan at higher energy levels indicated a gradual reduction in the hardness values with increasing energy density settings, though to varying degrees. The average hardness of the samples increased from single scan specimens having the lowest at 18.27 HRC to double scan with quarter energy density repetition specimens being the highest at 21.75 HRC. Double scan with half energy density repetition specimens showed most consistent hardness values across all energy density levels with an average of 20.16 HRC There is a distinct improvement from no re-melting to re-melting with the repeating energy density causing a sharp reheating of the already formed crystals and consequent sharp cooling. This results in an overall reduction in the size of grains, giving higher hardness values. Additionally, the hardness values of all three sets of SLM specimens proved to be superior over traditionally manufactured 316L stainless steel results.

4.4 Porosity

Porosity was identified as a crucial physical property to be rectified in SLM parts in order to be really qualified to replace the traditional counterparts. Fully dense metals with no defects and imperfections produce optimal physical and mechanical properties and re-melting was found to contribute to this desired result [16]. The porosity results obtained from samples printed with single and double scanning methods at four different base energy densities are presented

in **Fig. 4-4**. Again, the overall variation in the porosity levels noticed for different conditions is very small in comparison with the experimental errors.

Consideing the results of **Fig. 4-4** more closely, it may be noted that there is a slight reduction in porosity with the re-melted cases compared to the single scanning at the two lower energy settings. However, this has changed at the two higher energy settings as evident from the last two sets of bar graphs in **Fig. 4-4**. Though these changes are quite marginal, repeated sintering at relatively higher energy densities appear to be detrimental to the porosity probalby due to over heating and loss of the layer quality. At the highest energy density of 185 J/mm^3, the re-melting technique proved to be the most detrimental to the porosity compared to the single scanning results.

Overall, the average porosity is the highest in single scanning at 3.60 % and decreases with double scanning with half and quarter repetitions at 3.49 % and 3.38 %, respectively. The differences in the average values are minimal; however, the minimum percentage of porosity achieved with re-melting is 2.67 % and 2.68 % for double scan with half energy density repetition samples with energy density at 148 J/mm^3 and double scan with quarter energy density repetition samples with energy density at 110 J/mm^3, respectively, while the lowest porosity achieved by single scanning is 3.10 % at 148 J/mm^3.

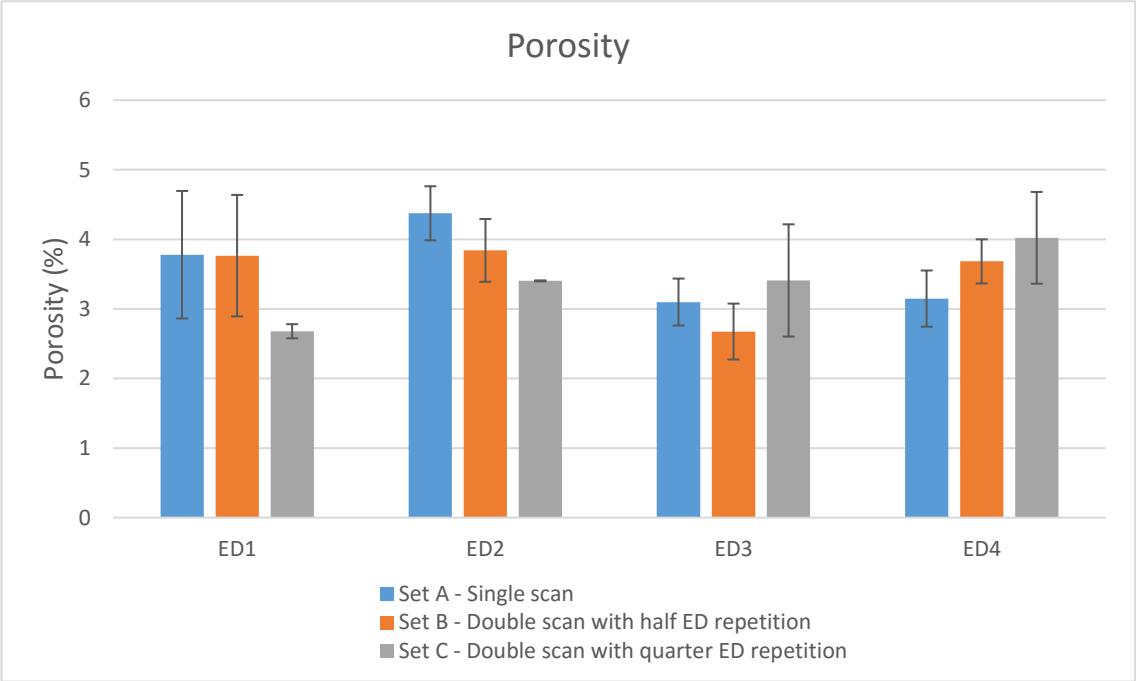

Fig. 4-4 - Porosity of SLM 316L stainless steel specimens

4.5 Surface roughness

The qualities of the top surfaces of the SLM 316L stainless steel specimens can be observed with the naked eye. There is a clear distinction between set A with no re-melting and sets B and C with re-melting. As shown in **Fig. 4-5**, samples of set A appear dull with an uneven texture and colour whereas samples of set C are more uniform and quite shiny. Usually, the first scan collects a set of particles and consolidates them into a layer with irregularities of varying degrees. Depending on the extent of phenomena such as balling, the surfaces resulting from the first scan are often quite irregular in forms as evident from the samples

of set A in **Fig. 4-5**. When laser re-melting is done on these surfaces, the additional heat energy from the repeating scans removes some of the irregularities. Also, the absence of fresh powder reduces the risk of burnishing and so the discolouring effects are diminished, eventually leading to the shiny, bright, and more uniform surfaces as seen in set C of **Fig. 4-5**.

Fig. 4-5 - Top surface quality comparison between set A and set C

As the differences in lateral surface qualities cannot be determined by simple visual examination, they are measured using the Taylor Hobson Talysurf discussed in Section 2.4.5. The results are as presented in **Fig. 4-6** which shows that the surface roughness of the lateral surfaces did not benefit much from re-melting every layer of the stainless steel specimens. The re-melted samples produced either almost similar or slightly inferior surface roughness values, with the average lateral surface roughness being 24.50 µm, 25.09 µm and 24.98 µm for set A, B and C, respectively.

With the laser revisiting the same layer again, the heat is reapplied, which may cause some of the surrounding powder particles to adhere to the outermost edges of the part as the build occurs within the powder bed. Also, the changes in

laser power and laser scan speed did not have a palpable effect on the lateral surface roughness. Typically, the surface roughness value range for the selectively laser melted metal parts is between 15 µm and 40 µm. The lateral surface roughness values of 316L stainless steel specimens, as shown in **Fig. 4-6**, fall within this range. Depending on the application and the desired surface finish for the final SLM product, post processing may be required for a smaller R_a.

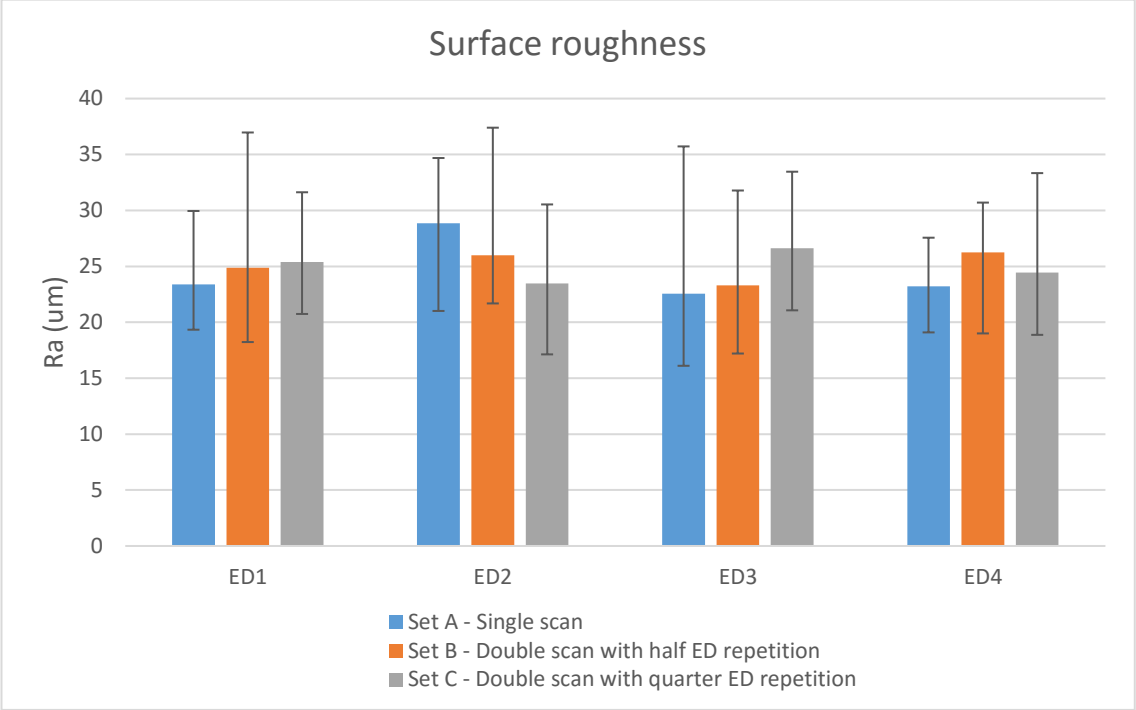

Fig. 4-6 - Lateral surface roughness of SLM 316L stainless steel specimens

Chapter 5
Results, discussion, and conclusions

5.1. The process-structure-property chain

The relational aspects from process to structure and then structure to property responses are vital to understand the consequences of the re-melting approach applied to selective laser melting. The experimental research allowed to evaluate light optical and scanning electron photomicrographs for changes in melt pool shapes, porosity and internal grain growth patterns of laser melted 316L stainless steel with and without re-melting. Selective laser re-melting is projected as a solution to reducing the balling phenomenon in SLM 316L stainless steel. If not attended to, balling directly leads to an increase in porosity. Every subsequent layer is affected as fresh powder material is not able to spread uniformly, leading to parts with low density and therefore inadequate mechanical and physical properties. Laser re-melting is expected to achieve full density in a part by eliminating melt pool borders and creating bigger melt pools for less fusion zones that are susceptible to cracks.

Based on the results of the experiments conducted, it appears that the differences between single and double pass laser scanning with varying energy density settings are not as spectacular as some studies have suggested earlier. However, there are notable observations and patterns in the results that are

presented in Chapters 3 and 4. These results are critically analysed identifying the process to structure and structure to property relationships in the following sections. Inferences are also drawn critiquing the claims made in the literature, where possible.

5.2. Process-structure relationships

Microstructural features in SLM 316L stainless steel vary with changes in process parameters and build strategies. These are observed using both light optical microscope and scanning electron microscope to obtain an in-depth overview of laser re-melting in terms of the formation of the melt pools and grain structures. The distinct and equi-sized melt pools as reported with the normal laser melting process are either elongated or enlarged further to the re-melting of each layer. Evidently, re-melting scans attempt to eliminate melt pool borders in order to consolidate laser scan tracks and layers, and reduce porosity to produce a fully dense part. The build parameters of double scanning with half energy density repetition are sufficient in creating horizontal layers that closely resemble the lamellar structure, but not to the extent of the extremely fine lamellar structure reported by Yasa *et al*. [16], due to the different build conditions.

In all three sets of samples with varying laser scan strategies, parallel growth of cellular dendritic cells is observed, while the dendrites are often angled towards the normal of the melt pool borders. This is due to the direction of maximum rate of heat transfer being perpendicular to the fusion line as the laser beam applies high local energy to the powder material and it solidifies against the substrate

layer. However, not all growth orientation follows the maximum heat flux direction as it is also affected by the preferred growth orientation related to the crystal structure [55].

A recent study has demonstrated a significant increase in the mean primary dendrite spacing in a SLM 316L stainless steel part with an increase in volume energy density [55]. With the minimum and maximum energy density settings at 104.17 J/mm^3 and 178.57 J/mm^3, the mean primary dendrite spacing was observed to increase from approximately 0.31 µm to 0.74 µm, respectively. Though the current evaluation has not considered the estimate of dendritic spacing, there is evidence that with re-melting, the intragranular cellular segregation network structures within the solidified columnar grains are more refined compared to the single scan cases.

The intragranular cellular segregation network structures within the dendrites are prominent throughout all samples with laser re-melting, and visible in some SLM samples built with higher energy density settings as evident from **Fig. 3-5 (ii)** and **3-6 (ii)**. The fine cellular substructures vary in shape with the maximum diameter not exceeding 10 µm, while the areas closer to fusion zones consist of deformed and / or slightly elongated intragranular cellular segregation network structures. With a large degree of undercooling and rapid cooling rates reaching up to approximately 10^7 K/s in SLM, as discussed in Chapter 3.3, the solidification process and resulting microstructural features are found to be similar to those produced in laser welded beads [56].

The selective laser re-melting technique is recognised as the best solution to eliminating open and trapped porosity in SLM 316L stainless steel parts. Yasa *et al*. reported almost fully dense parts with laser re-melting where they claimed to have achieved a difference between SLM part and the densest SLR part of 0.738 %; approximately 25 times less porosity for the re-melted parts [16]. The energy density of their re-melting scans vary greatly between 35 J/mm^3 to 283 J/mm^3 with 74 J/mm^3 as the base energy density common for all samples. It was concluded that any energy density used with re-melting produced significantly denser parts than normal SLM with no re-melting, irrespective of the number of re-melting scans used. In this study, the energy density levels for the repeated laser scans are varied according to the initial energy density settings and either half or quarter energy density levels are employed for the repeated scans. There are no clear patterns in terms of porosity with the initial energy density ranging from 110 J/mm^3 to 185 J/mm^3, and the re-melting energy density ranging from 27 J/mm^3 to 92 J/mm^3. While single pass laser scanning samples feature larger rounded pores, cracks along melt pool borders are visible in both single and double pass samples, as discussed in Section 3.3.

Sun *et al*. defined the melt track morphologies that are formed by different laser scanning strategies in relation to the build direction in an SLM build [57]. It was found that a combination of these scanning directions in a single build enabled the layers to adhere successfully with minimal residual stresses. This may be a plausible solution to cracks that form along fusion zones, which are present in both SLM and SLR samples as discussed in Section 3.3. It is likely that certain areas of solidified melt pools will undergo re-heating or re-melting along the different laser scanning directions. Further research is required to fully analyse

the effectiveness of applying combinations of laser scanning strategies along with the laser re-melting approaches.

5.3. Structure-property relationships

The mechanical and physical properties of SLM metal parts are heavily reliant on the microstructural features. Specifically, homogeneity in microstructure is crucial in producing uniform material properties [58]. However, the results from this study do not show a clear directly proportionate relationship between the density and other material properties as suggested in the literature. Overall, the double pass with quarter energy density repetition led to the best overall results. This could be explained by the range of energy density for the initial scans, as presented in **Table 3** and discussed in Section 2.5.2. These energy density values are the most appropriate for SLM 316L stainless steel without the use of the re-melting stage. While energy density settings ranging from 110 J/mm^3 to 185 J/mm^3 are ideal for SLM, it may be beneficial to decrease the initial energy density values for selective laser re-melting.

Meander laser scanning strategy, as defined in Section 2.5.4 is applied to print the dog bone tensile specimens, and is known to partially re-melt solidified melt pools of substrate layers [56]. This technique, in combination with the re-melting scans, means there is a possibility that the areas affected may undergo overheating, by being re-heated up to three times, and deteriorate the material. This was found to be true as the initial trials with re-melting at full energy density levels resulted in overheating and burnishing effects and complete loss of the

quality of the consolidated solid. As a result, the re-melting energy density levels are fixed at half and quarter energy levels compared to the settings used during the primary laser scanning. However, based on the porosity results as discussed in Chapter 4 it is felt that the half and the quarter energy density levels are also somewhat higher and so, the tensile test samples are printed with even lesser energy densities employed for the re-melting phase. It may be noted that the average tensile strength in 316L stainless steel increased from single scan to double scan even at the very low energy levels employed during the repeated melting of layers.

The build orientation appears to have a significant influence on the tensile strength. Samples built at an angle of 45° consistently gave the lowest tensile strength across all sets, while on the other hand, 0° samples gave the highest. This suggests that greater contact area with the substrate plate is optimal for a full consolidation of solidified scan tracks and layers. However, this is not always true and is heavily dependent on the geometrical complexities arising out of the necessity to provide additional support structures with overhanging surfaces. It was reported earlier that cellular lattice structures built at a strut angle of 45° were superior over those built with horizontal and vertical struts [59]. The struts that are oriented at 0° were almost impossible to manufacture due to severe overhanging. As the structural geometry becomes more complex, the build orientation has a greater effect on the material properties. For example, cellular lattice structures with dodecahedron based unit cell geometry are difficult to build as they contain a large number of horizontal and acute angle struts that lack support along their length [60].

The overall tensile strength benefitted from re-melting scans with low energy density settings. Furthermore, as discussed in Section 4.2, the samples built at a 90° showed the most improvement in tensile strength with re-melting. This suggests that components with thin walls will greatly benefit from laser re-melting. Considering the freedom to choose any combinations of process parameter settings, re-melting only the thin walled sections of a part is a possibility and also a viable option.

Density is also heavily dependent on SLM process parameters where higher laser scan speeds and smaller laser scan spacing were reported to have produced parts with lower porosities [57]. On the contrary, the results from this experiment show that lowest porosities were achieved with low laser power and laser scan speed while high laser power and laser scan speed are the contributing factors to the highest amount of porosity. Theoretically, low laser scan speeds would penetrate deeper into the material which creates melt pools with larger troughs. This is also evident to some extent in the light optical micrographs presented and discussed in Section 3.2. The contrasting results may be explained by the fact that although the study mentioned above used a laser power of 380 W, their range of laser scan speeds are much higher from 625 mm/s to 3000 mm/s, eventually giving low energy densities with a maximum energy density of 108.57 J/mm^3.

As mentioned in the previous section, Yasa *et al*. [16] claimed to have achieved almost fully dense laser re-melted parts of 98 % to 99 % relative densities. However, the method in which the density values were calculated is inaccurate, where three micrographs of each cross-sectional area were observed for

porosity. The micrographs were converted into black and white images for a ratio of pixels, then the calculated average of the three images was determined as the porosity in each sample. The absolute data, which is typically higher than true data, is unreliable as the results are merely a miniscule portion of the porosity within the part. The discrepancies between the current density levels obtained at an average of 96% compared the literature could be due to the differences in the measurement techniques.

5.4. Overall impressions

Overall, laser re-melting of every layer in SLM produces 316L stainless steel parts of higher quality than those with no re-melting due to a fuller consolidation of the melt pools, and reduced balling and porosity. Consequently, better mechanical and physical properties are achieved with the double pass laser scanning samples. Moreover, re-melting with quarter energy density levels produce better results than half energy density, possibly due to the high laser powers of the initial scans used in this study. Therefore, in selective laser re-melting builds with higher energy density settings with laser powers of 300 W to 400 W, it is recommended that full energy density is not applied to re-melting scans in order to prevent overheating and deterioration of the powder material.

Due to the numerous combinations of SLM process parameters, it is difficult to determine the exact resulting microstructural features. Further, the resulting mechanical and physical properties are inconsistent with other studies and hypotheses of re-melting in SLM indicating possible complications in the part

build, experimental methods and procedures. Further selective laser re-melting studies are required in order to produce more concrete conclusions on the true effects of the re-melting technique. Theoretically, high density in a SLM 316L stainless steel part means better material properties. However, this is disputable as it is not true for all cases presented in this re-melting study though the differences are minor. While SLM is a sensitive manufacturing process with the requirement to employ precise combinations of material and process parameters, selective laser re-melting has proven to be much more delicate as the re-melting scan parameters contribute greatly to the final part quality.

In terms of the commercial use, SLM technology has numerous competitive advantages that are superior over conventional manufacturing methods. However, it is yet inadequate in mass production due to its high cost per part characteristics. Also, while SLM boasts of the ability to produce complex geometries, even with the option of combining multiple parts into a single build, such diverse types of surfaces and build orientations lead to unpredictable part qualities. Real-time adjustment of process parameters during manufacturing was suggested earlier as a possible approach [34]. The re-melting approach investigated here is a similar solution elucidating clear benefits, but further process parameter optimisation is necessary to reap the full potential of the method.

5.5. Conclusions

In comparing the effects of re-melting each layer in the selective laser melting of 316L stainless steel, three sets of samples were built with single scanning, double scanning with half energy density repetition and double scanning with quarter energy density repetition. The microstructural features are studied using both light optical and scanning electron microscopes. For the investigation of mechanical and physical characteristics, the samples are tested for tensile strength, hardness, surface roughness and porosity. The general and the more specific conclusions drawn based on the results of the experimental investigations carried out are presented in the following sections.

5.5.1 General observations

Laser re-melting in SLM 316L stainless steel samples shows signs of elimination of melt pool boundaries. Double pass laser scanning samples produce bigger melt pools, where the half energy density repetition produces elongated melt pools, showing characteristics of the lamellar structure. The quarter energy density repetition of laser scanning led to enlarged melt pools that mirror the shape of the single scan samples. No clear variations in the melt pool formation patterns are noted in the single pass laser scan specimens with increasing energy density, as the size, shape and orientation of melt pools remained fairly consistent. The elongated melt pools in the double pass with half energy density repetition specimens became slightly rounded and inconsistent in thickness with increasing energy density. Finally, double pass with quarter energy density

repetition specimens produced melt pools comparable to those with no re-melting at low energy density settings. Both the height and the width of these melt pools also increased with increasing energy density. Melt pool widths varied greatly across all energy density settings and laser scan strategies.

The microstructures of the single pass laser scan specimens consisted of the microstructural features of the typical SLM 316L stainless steel part. Intragranular cellular segregation network structures are found in melt pools of both double pass with half and quarter energy density repetition specimens. Interlayer and inter border cells also have certain critical characteristics in the re-melted samples., The re-melting at the half energy density lead to probable recrystallisation and re-structuring of the cellular matrices close to the single pass forms. The quarter energy density repetition resulted in a camouflaged cellular structure with the grain boundaries erased at places. Large spherical pores and cracks are found along the melt pool borders in most samples. With increasing energy density, both the amount of grain growth in the build direction and porosity increased. Furthermore, the re-melted samples had less large pores than single pass laser scan specimens.

The dog bone tensile test specimens with no re-melting obtain greater elongation values (**Fig. 5-1**) but less tensile strength compared to those with re-melting. The small re-melting energy density settings improve the average tensile strength by approximately 10 MPa. Similarly, the build orientation that produced the greatest elongation has the lowest tensile strength, disregarding energy density and laser scan strategies, due to the staircase effects on the inclined surfaces. The 316L stainless steel parts built at 45° performed poorly compared to the horizontal and

vertical samples with a difference of approximately 36 MPa on the average tensile strength.

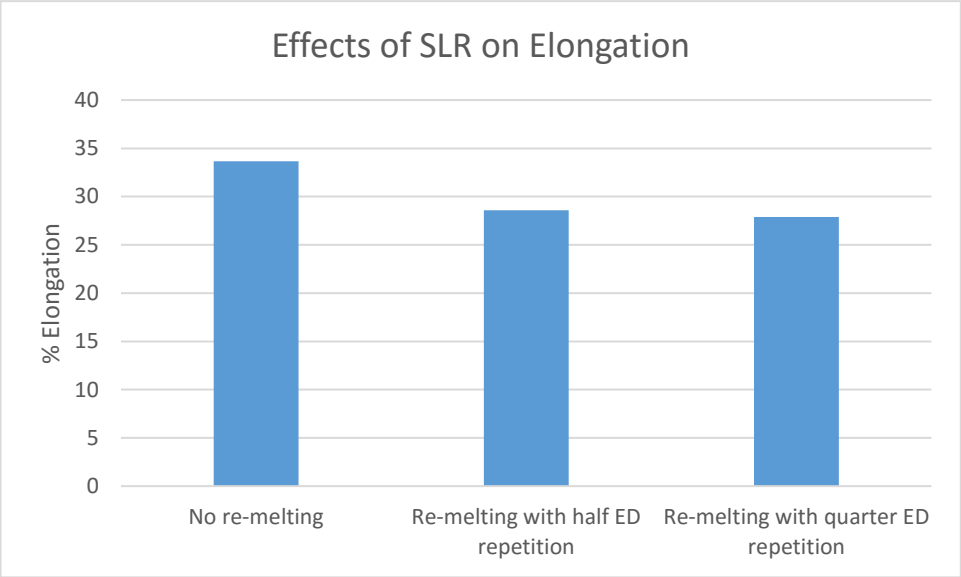

Fig. 5-1 – Effects of selective laser re-melting on elongation

The tensile test specimens built at an angle of 90° benefit the most with laser re-melting. The vertical orientation provides the smallest surface area in which the laser heat source comes in contact with, which allows the inter-layer bonding to be strengthened by the re-melting scans. The average values of hardness, porosity and top surface roughness results show that double pass with quarter energy density repetition specimens are superior over single pass and double pass with half energy density repetition specimens. The latter samples both decrease in hardness with increasing energy density while the first has a maximum hardness of 26 HRC at 148 J/mm^3. The highest energy density of 185 J/mm^3 prove to be detrimental for the single pass laser scan specimens, with no re-melting for full consolidation, which obtained the lowest hardness of 13 HRC.

The re-melting technique does assist in the reduction of porosity with the average percentage porosity decreasing from 3.60 % for single pass to 3.49 % and 3.38 %, for double pass with half energy density repetition and double pass with quarter energy density repetition, respectively. The energy density settings within the laser scan strategies do not appear to have much influence on porosity. Single pass specimens produced the most porosity at the energy density setting of 137 J/mm^3 and the lowest amount of porosity at 148 J/mm^3 and 185 J/mm^3. Double pass with half energy density repetition specimens have a similar pattern throughout the energy density settings with lowest amount of porosity at 148 J/mm^3, but appear to be consistent throughout the other energy density settings. On the other hand, double pass with quarter energy density repetition specimens produced an increasing amount of percentage porosity with increasing energy density.

Finally, the surface roughness values show that the re-melting technique is disadvantageous to the lateral surfaces of SLM 316L stainless steel parts. While the difference is miniscule, single pass specimens produced an average lateral surface roughness of 24.50 µm and double pass specimens give an approximate average value of 25.09 µm. The double pass laser scan specimens are fairly consistent throughout the varying energy density settings. The single pass specimens produced a pattern which emulates the porosity results, where the maximum surface roughness is found at an energy density of 137 J/mm^3.

5.5.2 Specific Quantitative Conclusions

To justify the efficacy of selective laser re-melting, AISI 316L stainless steel parts were built via SLM with the re-melting technique and varying energy density settings. The following are the more specific and quantitative conclusions drawn based on the experimental results:

- Selective laser re-melting with quarter energy density repetition is optimal for a successful build with 316L stainless steel when using high laser powers between 300 W to 400 W with density of up to 96.62 %. Better hardness, porosity and top surface roughness values are obtained with these settings, compared to those of single pass with no re-melting and double pass with half energy density repetition specimens.

- The heights of melt pools produced in single pass laser scan specimens ranged from approximately 30 µm to 80 µm while both double pass laser scan specimens produced larger melt pools with heights ranging between approximately 30 µm to 100 µm.

- A small re-melting energy density will aid in full consolidation of the powder material in SLM which improves tensile strength. The samples with double scanning obtained an average UTS of over 581 MPa which is greater than single scan samples by at least 10 MPa. On the other hand, single scan samples gave the highest percent elongation of 33.66 %, while re-melted samples ranged from approximately 27.87 % to 28.60 %.

- In terms of build orientation, the samples built at an angle of 45° produced the lowest UTS of 561.06 MPa, while the results for 0° and 90° samples were 597.36 MPa and 575.94 MPa.

- The double scan with quarter energy density samples produced the best results in hardness and porosity tests, the average values being 21.75 HRC, and 3.38 %, respectively. Similarly, the double scan with half energy density samples obtained a hardness value of 20.16 HRC and porosity of 3.49 %, and the single scan samples produced the worst with 18.27 HRC and 3.60 %, respectively.

- The lateral surface roughness was worse in double scan samples with R_a up to 25 µm. However, the effect of re-melting was not significant and post processing of the material is a possibility depending on the application of the SLM part.

References

[1] Kruth, J. P., Van Vaerenberg, J., Froyen, L., & Rombouts, M. . (2005). Binding mechanisms in selective laser sintering and selective laser melting. Rapid Prototyping Journal. , 11(1), 26-36.

[2] Van Elsen, M., Al-Bender, F., & Kruth, J. P. (2008). Application of dimensional analysis to selective laser melting. Rapid Prototyping Journal, 14(1), 15-22.

[3] Jia, T., Zhang, Y., & Chen, J. K. (2011). Dynamic simulation of particle packing with different size distributions. *Journal of Manufacturing Science and Engineering, 133*(2), 021011.

[4] Zhou, J., Zhang, Y., & Chen, J. K. (2009). Numerical simulation of random packing of spherical particles for powder-based additive manufacturing. *Journal of Manufacturing Science and Engineering, 131*(3), 031004.

[5] Rickenbacher, L., Spierings, A., & Wegener, K. (2013). An integrated cost-model for selective laser melting (SLM). Rapid Prototyping Journal, 19(3), 208-214.

[6] Gu, D. D., Meiners, W., Wissenbach, K., & Poprawe, R. (2012). Laser additive manufacturing of metallic components: materials, processes and mechanisms. . International Materials Reviews, 57(3), 133-164.

[7] Niu, H. J., & Chang, T. H. (2000). Selective laser sintering of gas atomized M2 high speed steel powder. Journals of Materials Science, 35, 31-38.

[8] Simchi, A. (2006). Direct laser sintering of metal powders: Mechanism, kinetics and microstructural features. . Materials Science and Engineering A, 428, 148-158.

[9] Badrossamay, M., & Childs, T. H. C. (2006). Layer Formation Studies in Selective Laser Melting of Steel Powders. Proceedings of 17th Solid Freeform Fabrication Symposium, Austin, Texas, USA.

[10] Childs, T. H. C., Hauser, C., & Badrossamay, M. (2005). Selective laser sintering (melting) of stainless and tool steel powders: experiments and modelling. Proceedings of the Institution of Mechanical Engineers, Part B: Journal of Engineering Manufacture, 219(4), 339-357.

[11] Joo, B. D., Jang, J. H., Lee, J. H., Son, Y. M., & Moon, Y. H. (2009). Selective laser melting of Fe-Ni-Cr layer on AISI H13 tool steel. Transactions of Nonferrous Metals Society of China, 19(4), 921-924.

[12] Liu, Z. H., Chua, C. K., Leong, K. F., Kempen, K., Thijs, L., Van-Humbeeck, J., & Kruth J. P. (2011). A preliminary investigation on Selective Laser Melting of M2 high speed steel. Paper presented at the Innovative Developments in Virtual and Physical Prototyping: Proceedings of the 5th International Conference on Advanced Research in Virtual and Rapid Prototyping.

[13] Liu, Z. H., Zhang, D. Q., Chua, C. K., & Leong, K. F. (2013). Crystal structure analysis of M2 high speed steel parts produced by selective laser melting. Materials Characterization, 84, 72-80.

[14] Benyounis, K. Y., Fakron, O. M., & Abboud, J. H. (2009). Rapid solidification of M2 high-speed steel by laser melting. Materials & Design, 30(3), 674-678.

[15] Kac, S., & Kusinski, J. (2003). SEM and TEM microstructural investigation of high-speed tool steel after laser melting. Materials Chemistry and Physics, 81, 510-512.

[16] Yasa, E., Deckers, J., & Kruth, J. P. (2011). The investigation of the influence of laser re-melting on density, surface quality and microstructure of selective laser melting parts. Rapid Prototyping Journal, 7(5), 312-327.

[17] Strano, G., Hao, L., Everson, R. M., & Evans, K. E. (2013). Surface roughness analysis, modelling and prediction in selective laser melting. Journal of Materials Processing Technology, 213, 589-597.

[18] Yadroitsev, I., & Smurov, I. (2011). Surface morphology in selective laser melting of metal powders. Physics Procedia, 12, 264-270.

[19] Cherry, J. A., Davies, H. M., Mehmood, S., & Lavery, N. P. (2015). Investigation into the effect of process parameters on microstructural and physical properties of 316L stainless steel parts by selective laser melting. International Journal of Advanced Manufacturing Technology, 76, 869-879.

[20] Dudek, A., Wronska, A., & Adamczyk, L. (2014). Surface remelting of 316L + 434L sintered steel: microstructure and corrosion resistance. Journal of Solid State Electrochemistry, 18, 2973-2981.

[21] Airbaey, K., Wimpenny, D., Tosi, R., Manning, W., & Moroz, A. (2014). On optimization of surface roughness of selective laser melted stainless steel parts: a statistical study. Journal of Materials Engineering and Performance, 23, 2139-2148.

[22] Liu, B., Wildman, R., Tuck, C., Ashcroft, I., & Hague, R. (2011). Investigation the effect of particle size distribution on processing parameter optimisation in selective laser melting process. Paper presented at the International solid freeform fabrication symposium: an additive manufacturing conference, University of Texas at Austin, Austin.

[23] Brodin, H., Andersson, O., & Johansson, S. (2013). Mechanical behaviour and microstructure correlation in a selective laser melted superalloy. Paper presented at the ASME Turbo Expo 2013: Turbine Technical Conference and Exposition.

[24] Hanzel, P., Zetek, M., Baksa, T., & Kroupa, T. (2015). The influence of processing parameters on the mechanical properties of SLM parts. Procedia Engineering, 100, 1405-1413.

[25] Yadollahi, A., Shamsaei, N., Thompson, S. M., & Seely, D. W. (2015). Effects of process time interval and heat treatment on the mechanical and microstructural properties of direct laser deposited 316L stainless steel. Materials Science & Engineering A, 664, 171-183.

[26] Song, B., Dong, S., Deng, S., Liao, H., & Coddet, C. (2014). Microstructure and tensile properties of iron parts fabricated by selective laser melting. Optics & Laser Technology, 56, 451-460.

[27] Zhang, B., Dembinski, L., & Coddet, C. (2013). The study of the laser parameters and environment variables effect on mechanical properties of high compact parts elaborated by selective laser melting 316L powder. *Materials Science & Engineering A, 584*, 21-31.

[28] Zhou, X., Liu, X., Zhang, D., & Liu, W. (2015). Balling phenomena in selective laser melted tungsten. *Journal of Materials Processing Technology, 222*, 33-42.

[29] Yadroitsev, I., Krakhmalev, P., Yadroitsava, I., Johansson, S., & Smurov, I. (2013). Energy input effect on morphology and microstructure of selective laser melting single track from metallic powder. *Journal of Materials Processing Technology, 213*, 606-613.

[30] Delgado, J., Ciurana, J., & Rodriguez, C. A. (2012). Influence of process parameters on part quality and mechanical properties for DMLS and SLM with iron-based materials. International Journal of Advanced Manufacturing Technology, 60, 601-610.

[31] Guan, K., Wang, Z., Gao, M., Li, X., & Zeng, X. (2013). Effects of processing parameters on tensile properties of selective laser melted 304 stainless steel. Materials and Design, 50, 581-586.

[32] Li, R., Liu, J., Shi, Y., Du, M., & Xie, Z. (2010). 316L stainless steel with gradient porosity fabricated by selective laser melting. Journal of Materials Engineering and Performance, 19, 666-671.

[33] Miranda, G., Faria, S., Bartolomeu, F., Pinto, E., Madeira, S., Mateus, A., . . . Carvalho, O. (2016). Predictive models for physical and mechanical properties of 316L stainless steel produced by selective laser melting. *Materials Science & Engineering A, 657*, 43-56.

[34] Wang, D., Liu, Y., Yang, Y., & Xiao, D. (2016). Theoretical and experimental study on surface roughness of 316L stainless steel metal parts obtained through selective laser melting. *Rapid Prototyping Journal, 22*(4), 706-716.

[35] Pyka, G., Kerckhofs, G., Papantoniou, I., Speirs, M., Schrooten, J., & Wevers, M. (2013). Surface roughness and morphology customization of additive manufactured open porous Ti6Al4V structures. *Materials & Design, 6*, 4737-4757.

[36] Mercelis, P., Kruth, J. P. (2006). Residual stresses in selective laser sintering and selective laser melting. *Rapid Prototyping Journal, 12*(5), 254-265.

[37] Simonelli, M., Tuck, C., Aboulkhair, N. T., Maskery, I., Ashcroft, I., Wildman, R. D., & Hague, R. (2015). A study on the laser spatter and the oxidation reactions during selective laser melting of 316L stainless steel, Al-Si10-Mg, and Ti-6Al-4V. *Metallurgical and Materials Transactions A, 46*(9), 3842-3851.

[38] Frazier, W., E. (2014). Metal Additive Manufacturing: A Review. *Journal of Materials Engineering and Performance, 23*(6), 1917-1928.

[39] Dawes, J., Bowerman, R., & Trepleton, R. (2015). Introduction to the additive manufacturing powder metallurgy supply chain. *Johnson Matthey Technology Review, 59*(3), 243.

[40] Dadbakhsh, S., Hao, L., & Sewell, N. (2012). Effect of selective laser melting layout on the quality of stainless steel parts. *Rapid Prototyping Journal, 18*(3), 241-249.

[41] Li, R., Shi, Y., Wang, Z., Wang, L., Liu, J., & Jiang, W. (2010). Densification behaviour of gas and water atomized 316L stainless steel powder during selective laser melting. *Applied Surface Science, 256*, 4350-4356.

[42] Khairallah, S. A., Anderson, A. T., Rubenchik, A., & King, W. E. (2016). Laser powder-bed fusion additive manufacturing: Physics of complex melt flow and formation mechanisms of pores, spatter, and denudation zones. *Acta Materialia, 108*, 36-45.

[43] Laroudie, F., Tassin, C., & Pons, M. (1995). Hardening of 316L stainless steel by laser surface alloying. *Journal of Materials Science, 30*(14), 3652-3657.

[44] Tassin, C., Laroudie, F., Pons, M., & Lelait, L. (1996). Improvement of the wear resistance of 316L stainless steel by laser surface alloying. *Surface and Coatings Technology, 80*, 207-210.

[45] Kwok, C. T., Lo, K. H., Cheng, F. T., & Man, H. C. (2003). Effect of processing conditions on the corrosion performance of laser surface-melted AISI 440C martensitic stainless steel. *Surface and Coatings Technology, 166*, 211-230.

[46] Arias, J., Cebeza, M., Castro, G., Feijoo, I., Merino, P., & Pena, G. (2010). Microstructural characterization of laser surface melted AISI M2 tool steel. *Journal of Microscopy, 239*(3), 184-193.

[47] Carboni, C., Peyre, P., Beranger, G., & Lemaitre, C. (2002). Influence of high power diode laser surface melting on the pitting corrosion resistance of type 316L stainless steel. *Journal of Materials Science, 37*, 3715-3723.

[48] Yasa, E., & Kruth, J. P. (2011). Application of laser re-melting on selective laser melting parts. *Advances in Production Engineering & Management, 6*(4), 259-270.

[49] Mumtaz, K., & Hopkinson, N. (2009). Top surface and side roughness of Inconel 625 parts processed using selective laser melting. *Rapid Prototyping Journal, 15*(2), 96-103.

[50] Zhong, Y., Liu, L., Wikman, S., Cui, D., & Shen, Z. (2016). Intergranular cellular segregation network structure strengthening 316L stainless steel prepared by selective laser melting. *Journal of Nuclear Materials, 470*(170-178).

[51] Glicksman, M. E. (2010). Principles of solidification: an introduction to modern casting and crystal growth concepts: Springer Science & Business Media.

[52] Fredriksson, H., & Akerlind, U. (2012). Solidification and crystalization processing in metals and alloys: John Wiley & Sons.

[53] Saeidi, K., Gao, X., Zhong, Y., & Shen, Z. J. (2015). Hardened austenite steel with columnar sub-grain structure formed by laser melting. *Materials Science & Engineering A, 625*, 221-229.

[54] Thijs, L., Sistiaga, M. L. M., Wauthle, R., Xie, Q., Kruth, J. P., & Van Humbeeck, J. (2013). Strong morphological and crystallographic texture and resulting yield strength anisotropy in selective laser melted tantalum. *Acta Materialia, 61*(12), 4657-4668.

[55] Wang, D., Song, C., Yang, Y., & Bai, Y. (2016). Investigation of crystal growth mechanism during selective laser melting and mechanical property characterization of 316L stainless steel parts. *Materials and Design, 100*, 291-299.

[56] Casati, R., Lemke, J., & Vedani, M. (2016). Microstructure and fracture behavior of 316L austenitic stainless steel produced by selective laser melting. *Journal of Materials Science and Technology, 32*, 738-744.

[57] Sun, Z., Tan, X., Tor, S. B., & Yeong, W. Y. (2016). Selective laser melting of stainless steel 316L with low porosity and high build rates. *Materials and Design, 104*, 197-204.

[58] Dutta Majumdar, J., Pinkerton, A., Liu, Z., Manna, I., & Li, L. (2005). Microstructure characterisation and process optimization of laser assisted rapid fabrication of 316L stainless steel. *Applied Surface Science, 247*, 320-327.

[59] Yan, C., Hao, L., Hussein, A., Young, P., & Raymont, D. (2014). Advanced lightweight 316L stainless steel cellular lattice structures fabricated via selective laser melting. *Materials and Design, 55*, 533-541.

[60] Mullen, L., Stamp, R. C., Brooks, W. K., Jones, E., & Sutcliffe, C. J. (2009). Selective laser melting: a regular unit cell approach for the manufacture of porous, titanium, bone in-growth constructs, suitable for orthopedic applications. *Journal of Biomedical Materials Research Part B: Applied Biomaterials, 89B*(2), 325-334.

POSTGRADUATE

AUT

FORM PGR16 APPLICATION FOR RESTRICTED ACCESS TO A THESIS/DISSERTATION/EXEGESIS

PLEASE NOTE

- *This form must be typed. Handwritten forms will not be accepted.*
- *Double clicking on the check boxes enables you to change them from not-checked to checked.*
- *The completed form, signed by the student and the primary supervisor, should be submitted to the appropriate Faculty Postgraduate Office when the thesis/exegesis is lodged for examination. If the application is approved by the Faculty Postgraduate Committee, the form will be signed by the Dean and sent to the University Postgraduate Centre for insertion into the print copies deposited. For more information consult the Postgraduate Handbook.*

Student ID No	1107415	**Name**	Sonia Chung
Faculty	DCT	**School/Dept**	School of Engg Computing and Mathematical Sciences
Programme	Master of Engineering	**Date of submission for examination**	January 2017
Research Output	**Thesis** ☒ **Dissertation** ☐	**Exegesis** ☐	**Points Value** 120
Thesis Title	Selective Laser Re-melting		

EMBARGO TIMEFRAME

An embargo is requested on the public availability of the print and digital copies of the above thesis/exegesis from the date of submission for examination (maximum normally 36). **24** **months**

EMBARGO CATEGORIES

The thesis/dissertation/exegesis contains confidential or sensitive information which if publicly available may *(Tick all that apply)*

☒ Jeopardise the future intellectual property rights of the author (e.g. a patent application or publication)

☐ Breach a prior contractual arrangement with an external organisation *(Please attach a copy of the relevant agreement(s))*

☐ Infringe or endanger the right to privacy or cultural respect of an individual or group

The embargo would apply to

☒ The complete thesis/dissertation/exegesis

☐ A portion of the work (specify) :

Signatures

Student	Sonia Chung	**Signature**		**Date**	20-12-2016
Primary Supervisor	Assoc Prof Sarat Singamneni	**Signature**		**Date**	20-12-2016
Secondary Supervisor	Prof. Thomas Neitzert	**Signature**	Thomas Neitzert	**Date**	09-01-2017
Additional Supervisor/Mentor		**Signature**		**Date**	

RESTRICTED ACCESS APPROVED BY FACULTY DEAN (or delegate)

Signature Rosser Johnson

Digitally signed by Rosser Johnson
DN: cn=Rosser Johnson, o=AUT, ou=DCT Faculty Office, email=rjohnson@aut.ac.nz, c=NZ
Date: 2017.03.01 14:55:03 +13'00'

Date

OFFICE USE

Expires 21 MAR 2019 KH.

POSTGRADUATE

AUT

FORM PGR16 APPLICATION FOR RESTRICTED ACCESS TO A THESIS/DISSERTATION/EXEGESIS

PLEASE NOTE

- *This form must be typed. Handwritten forms will not be accepted.*
- *Double clicking on the check boxes enables you to change them from not-checked to checked.*
- *The completed form, signed by the student and the primary supervisor, should be submitted to the appropriate Faculty Postgraduate Office when the thesis/exegesis is lodged for examination. If the application is approved by the Faculty Postgraduate Committee, the form will be signed by the Dean and sent to the University Postgraduate Centre for insertion into the print copies deposited. For more information consult the Postgraduate Handbook.*

Student ID No	1107415	**Name**	Sonia Chung
Faculty	DCT	**School/Dept**	School of Engg Computing and Mathematical Sciences
Programme	Master of Engineering	**Date of submission for examination**	January 2017
Research Output	**Thesis** ☒ **Dissertation** ☐	**Exegesis** ☐	**Points Value** 120
Thesis Title	Selective Laser Re-melting		

EMBARGO TIMEFRAME

An embargo is requested on the public availability of the print and digital copies of the above thesis/exegesis from the date of submission for examination (maximum normally 36). **24** **months**

EMBARGO CATEGORIES

The thesis/dissertation/exegesis contains confidential or sensitive information which if publicly available may *(Tick all that apply)*

☒ Jeopardise the future intellectual property rights of the author (e.g. a patent application or publication)

☐ Breach a prior contractual arrangement with an external organisation *(Please attach a copy of the relevant agreement(s))*

☐ Infringe or endanger the right to privacy or cultural respect of an individual or group

The embargo would apply to

☒ The complete thesis/dissertation/exegesis

☐ A portion of the work (specify) :

Signatures

Student	Sonia Chung	**Signature**		**Date**	20-12-2016
Primary Supervisor	Assoc Prof Sarat Singamneni	**Signature**		**Date**	20-12-2016
Secondary Supervisor	Prof. Thomas Neitzert	**Signature**	Thomas Neitzert	**Date**	09-01-2017
Additional Supervisor/Mentor		**Signature**		**Date**	

RESTRICTED ACCESS APPROVED BY FACULTY DEAN(or delegate)

Signature Rosser Johnson Digitally signed by Rosser Johnson DN: cn=Rosser Johnson, o=AUT, ou=DCT Faculty Office, email=rjohnson@aut.ac.nz, c=NZ Date: 2017.02.13 15:03:53 +13'00' **Date**

OFFICE USE **RELEASE DATE**